Asymptotic Analysis of a Wntβ-catenin pathway model

Postgraduate Programm: Computational Mechanics

Dimitris Maris

Advisor: Prof. Dimitris Goussis

Mechanics Section
School of Applied Mathematical and Physical Science
National Technical University of Athens

Athens
November 2014

Abstract

The *Wnt/β-catenin* signaling pathway is a signal transduction pathway made of proteins that pass signals inside the cell, through the receptors at its surface, and plays an important role in oncogenesis and development. Ethan Lee and his team introduced in 2003 a detailed mathematical model of the *Wnt/β-catenin* signal transduction pathway, consisting of a system of 15 differential equations. Their model incorporates the kinetics of protein-protein interactions, protein synthesis/degradation, and phosphorylation/dephosphorylation. Here, the fast/slow dynamics of *Lee et al.* system will be analyzed, by employing the *Computational Singular Perturbation (CSP)* algorithm. Given a multi-scale (stiff) N-dim. system of ordinary differential equations which exhibits M fast time scales, the solution is attracted quickly on a $N - M$ *Slow Invariant Manifold (SIM)*. On the *SIM* the evolution of the process is governed by a system, which is free of the fast time scales, so that the flow there is characterized by the slow time scales. The *CSP* algorithm provides an approximation of the *SIM* and of the slow system. A number of *CSP*-related *diagnostic tools* are employed for the analysis of the *Wnt/β-catenin* model, which provide all the relevant physical understanding for the function of the *Wnt/β-catenin* signaling pathway. The purpose of the present analysis is to identify the components (reactions) of the *Wnt/β-catenin* signaling pathway that (i) generate the fast time scales, (ii) participate in the formation of the *SIM* and (iii) drive the system on the *SIM*.

Contents

1 Introduction **7**

2 The CSP algorithm **11**
2.1 Implementation of the CSP refinements 14
2.1.1 Phase (1) of the *CSP* refinements 14
2.1.2 Phase (2) of the *CSP* refinements 16
2.1.3 Time derivatives of the Jacobian 17
2.2 The Criteria to identify the M number of the exhausted modes 18
2.2.1 First order accuracy 18
2.2.2 Second order accuracy 18
2.3 The CSP diagnostic tools 19
2.3.1 The CSP Pointer 19
2.3.2 The Participation Index 19
2.3.3 The Importance Index 20
2.3.4 The Eigenvalue Participation Index 20

3 The Wnt/β-catenin signaling pathway **23**
3.1 The Wnt/β-catenin signaling model 25
3.2 The dynamics of the *Wnt* model 30

4 CSP analysis on the *Wnt/β model* **33**
4.1 The reference state 33
4.1.1 One exhausted mode 34
4.1.2 Two exhausted modes 36
4.1.3 Three exhausted modes 38
4.1.4 Four exhausted modes 40
4.2 The stimulated state 43
4.2.1 One exhausted mode 44
4.2.2 Two exhausted modes 46
4.2.3 Three exhausted modes 48
4.2.4 Four exhausted modes 51
4.2.5 Five exhausted modes 53

5 Conclusions **57**

Chapter 1

Introduction

The biological mechanisms that are currently of interest are usually very complex, in which case the acquisition of the relevant physical understanding can be a very demanding task. The need to acquire this knowledge has directed biology into a more mathematical/computational approach [15]. The results produced with this approach and their comparison to experimental ones can be very useful since:

- the generation of new data that are not yet extrapolated from experiments is allowed,
- *in silico* "experiments" can be performed to save time and money,
- non-intuitive insights can be obtained into the way these systems work,
- it is possible to identify missing parameters, components or functions in a system,
- it enables the visualization of the mechanisms studied.

One of the major difficulties in the simulation of cellular processes is to determine the values of the kinetic constants, because some of these constants are hard or even impossible to be derived from experiments. Therefore, assumptions are usually made in order to obtain numerical values for these constants. Such assumptions can be validated in the cases where the relevant physical understanding is available. The present work will address the need to acquire algorithmically the underlying physics of cellular processes that are modeled by complex multi-scale mathematical systems.

Cellular processes are usually modeled with the use of *Ordinal Differential Equation (ODE)* or *Partial Differential Equation (PDE)* systems [43]. The simulation of protein signal transduction or metabolism mechanisms, which are based on mass action and *Michaelis-Menten (MM)* kinetics, is usually based in *ODE* systems. These systems are (i) easy to handle due to their well understood mathematical framework, (ii) very fast, so they can be used to describe very large mechanisms, (iii) mathematically robust and (iv) more easy to handle than *PDE* systems [28].

Here, the Wnt/β-catenin signaling pathway will be considered, as it is modeled by a multi-scale system of ODEs. Its meaningful physical understanding will be sought by employing an algorithmic methodology that performs asymptotic analysis.

The Wnt/β-catenin signaling pathway is a signal transduction pathway consisting of proteins that pass signals outside of a cell, through the cell surface receptors, to the inside of the cell. The Wnt/β-catenin signaling pathway is well known in the biology community due to its involvement to differentiation, tissue development and its important role in oncogenesis. Wnt/β-catenin signaling pathway plays an important role to some kinds of cancers, such as colorectal cancer [7, 32] and in stem-cell maintenance [4, 32].

The Wnt/β-catenin signaling pathway was hard to model, due two lack of quantitive experimental data. As a result, the mathematical modeling research that has been completed so far is limited, when considering the biological importance of this pathway. The way the scientific community thought about the function of this pathway changed completely when Lee et al. [25] published a detailed *ODE* model, which could reproduced to a large extend the available experimental results [37]. This model incorporates the kinetics of protein-protein interactions, protein synthesis/degradation and phosphorylation/dephosphorylation. Numerical results produced with this model have been experimental verified, so the mathematical modeling research is based upon this detailed model. It has been analyzed extensively, by studying its robustness [12, 19] and by constructing reduced models [29].

One of the most important challenges regarding the *Wnt* pathway is to identify its components that are responsible for the creation and the regulation of the major dynamic characteristics of the model. This will be the focus of the current investigation.

Models representing *multi-scale* biochemical networks, such as the *Wnt* pathway, are usually non-linear and complex, making the interpretation of their dynamics a difficult task [36]. Due to the generated equilibria between the fast components of such models, their long term evolution is determined by the slower components of the system [18]. The identification of these components is a very important step, since they generate and regulate the long term dynamics and response of the model.

The traditional tool for the identification of the fast components of a multi-scale system and of the reduced model that drives its slow evolution is the emphSingular Perturbation Analysis (SPA). SPA is a tool that identifies (i) the fast components that participate in the various equilibrations that develop and (ii) the slow components that finally drive the system [14, 40, 41]. The disadvantage of the paper/pencil *SPA* is that it can handle relative simple models because it requires (i) the governing equations of the system to be cast in the proper non-dimensional form, (ii) the identification of the fast and the slow variables and (iii) the identification of the small parameter ϵ, which is indicative of the gap between the fast and slow time scales. Given the complexity of biological systems, the application of the *SPA* faces significant obstacles, mainly due to the complexity and size of the models that are currently of interest..

The fast/slow dynamics of Lee's system will be examined here, by employing the *Computational Singular Perturbation (CSP)* algorithm. *CSP* reproduces the results of the classical SPA in an algorithmic fashion. The methodology is not hindered by the size and complexity of the mathematical model and does not require the system to be cast in a dimensionless form. *CSP* identifies (i) the fast and slow variables, (ii) the equilibrations that developing under the action of the fast time scales, (iii) the reduced model that governs the slow evolution under the constraints (i.e., equilibria) generated by the fast time scales, and (iv) the components that contribute to the equilibria and the slow evolution [22, 23]. It will be shown that the detailed *ODE* model of *Lee et*

al. is amenable to further reduction, beyond the four Partial Equilibrium approximations (PEAs) employed in [25]. The number of the new equilibria that develop will be identified, as the system evolves in time, along with the components of the system that are responsible the most for their development.

First, the *CSP* methodology will be briefly presented and the *CSP* tools will be discussed. Next, the *Wnt* pathway will be introduced and some biological processes within the pathway will be discussed. The detailed model of *Lee et al.* will be then presented, along with its kinetic parameters, initial conditions and reaction rates. The results of the *CSP* analysis will be finally presented and discussed.

Chapter 2

The CSP algorithm

The success of *CSP* in the analysis of multi-scale systems is based on the existence of a time scale gap among the fastest timescales in the dynamics of the system and the timescale that is characteristic of the system's evolution. When these, say M, fast time scales are of dissipative nature (i.e., they are generated by processes that tend to drive the system to equilibrium) they become quickly exhausted, so that the fastest time scale of the slow ones becomes the characteristic time scale for the system's evolution. The gap between the slowest of the fast (τ_M) and the fastest of the slow (τ_{M+1}) time scales measures the time scale gap that is indicative of the fast/slow separation. This gap is approximated by the ratio:

$$\epsilon = \tau_M / \tau_{M+1} \tag{2.1}$$

which by definition satisfies $\epsilon < 1$.

Consider a physical process which is governed by the N-dimensional system of (*ODE*'s):

$$\frac{d\mathbf{y}}{dt} = \mathbf{g}(\mathbf{y}) \tag{2.2}$$

where $\mathbf{y}$ and $\mathbf{g}(\mathbf{y})$ are the N-dimensional column *state vector* and *vector field*, respectively and $\mathbf{g}$ is an algebraic function of $\mathbf{y}$. Let the dynamics of this system exhibit M dissipative time scales, which are much faster than the time scale that characterizes the evolution of the system. Such a system is known as a *stiff* one [1]. According to the *CSP* algorithm, the vector field $\mathbf{g}$ can be decomposed in a fast and a slow part, as:

$$\frac{d\mathbf{y}}{dt} = \mathbf{a}_r \mathbf{f}^r + \mathbf{a}_s \mathbf{f}^s \tag{2.3}$$

where $\mathbf{a}_r \mathbf{f}^r$ and $\mathbf{a}_s \mathbf{f}^s$ are the components of the vector field $\mathbf{g}(\mathbf{y})$ in the M-dimensional *fast subspace* and $N - M$ dimensional *slow subspace*, respectively. The fast subspace, where the fast time scales act, is spanned by the M $\mathbf{a}_i$ $(i = 1, ..., M)$ column vectors which form the $(N \times M)$ matrix $\mathbf{a}_r$:

$$\mathbf{a}_r = \Big[\mathbf{a}_1 \ \mathbf{a}_2 \ ... \ \mathbf{a}_M\Big] \tag{2.4}$$

The slow subspace, where the slow time scales act, is spanned by the $N-M$ $\mathbf{a}_j$ $(j=M+1,...,N)$ column vectors, which form the $N\times(N-M)$ matrix $\mathbf{a}_s$:

$$\mathbf{a}_s=\Big[\mathbf{a}_{M+1}\ \mathbf{a}_{M+2}\ ...\ \mathbf{a}_N\Big] \tag{2.5}$$

The *CSP* amplitudes $\mathbf{f}^r$ and $\mathbf{f}^s$ are the projections of the vector field $\mathbf{g}(\mathbf{y})$ in the M along the M fast and $N-M$ slow directions, respectively, and are defined by the relations:

$$\mathbf{f}^r=\mathbf{b}^r\mathbf{g}\qquad\qquad \mathbf{f}^s=\mathbf{b}^s\mathbf{g} \tag{2.6}$$

where

$$\mathbf{b}^r=\begin{bmatrix}\mathbf{b}^1\\ \mathbf{b}^2\\ :\\ \mathbf{b}^M\end{bmatrix}\qquad\qquad \mathbf{b}^s=\begin{bmatrix}\mathbf{b}^{M+1}\\ \mathbf{b}^{M+2}\\ :\\ \mathbf{b}^N\end{bmatrix} \tag{2.7}$$

The N-dimensional row vectors $\mathbf{b}^i$ $(i=1,...,N)$ are dual to the N-dimensional column vectors $\mathbf{a}_i$ $(i=1,...,N)$ and due to orthogonality they satisfy relations (2.8):

$$\mathbf{b}^r\mathbf{a}_r=\mathbf{I}^r_r\qquad \mathbf{b}^r\mathbf{a}_s=\mathbf{0}^r_s\qquad \mathbf{b}^s\mathbf{a}_r=\mathbf{0}^s_r\qquad \mathbf{b}^s\mathbf{a}_s=\mathbf{I}^s_s\qquad \mathbf{a}_r\mathbf{b}^r+\mathbf{a}_s\mathbf{b}^s=\mathbf{I}^N_N \tag{2.8}$$

where $\mathbf{I}^N_N$ and $\mathbf{0}$ are the unit $(N\times N)$ and zero $(M\times k)$ matrices respectively.

When the trajectory evolves on the $(N-M)$-dim. *SIM* the M fast dissipative time scales τ_i $(i=1,\ldots,M)$ are exhausted, so that the flow is characterized by the slow time scale τ_{M+1}. On the *SIM* the vector field $\mathbf{g}(\mathbf{y})$ has no component in the fast subspace; i.e., the amplitudes (2.9) attain negligible values:

$$\mathbf{f}^r=\mathbf{b}^r\bullet\mathbf{g}\approx\mathbf{0}^r \tag{2.9}$$

so that the flow on the *SIM* is approximated by the system:

$$\frac{d\mathbf{y}}{dt}\approx\mathbf{a}_s\mathbf{f}^s \tag{2.10}$$

Equation (2.10) results from the full system, Eq. (2.3), after neglecting the fast component. Therefore, this equation is non-stiff.

Note that since $\mathbf{a}_s\mathbf{b}^s=\mathbf{I}^N_N-\mathbf{a}_r\mathbf{b}^r$, Eqs. (2.9, 2.10) show that for the construction of both the algebraic equation approximating the manifold and the slow system, it is sufficient to have available the fast basis vectors $\mathbf{a}_r$ and $\mathbf{b}^r$ only.

The *CSP* basis vectors $\mathbf{a}_r$ and $\mathbf{a}_s$, and their duals $\mathbf{b}^s$ and $\mathbf{b}^r$ are approximated with the *CSP* algorithm by two iterative procedures, the "$\mathbf{b}^r$" and the "$\mathbf{a}_r$" *CSP* refinements. The $\mathbf{b}^r$-refinement alters $\mathbf{b}^r$ and $\mathbf{a}_s$, leaving $\mathbf{b}^s$ and $\mathbf{a}_r$ unaffected, and it is related to the accuracy in the description of the manifold [20, 21, 23, 44]. The $\mathbf{a}_r$-refinement alters $\mathbf{a}_r$ and $\mathbf{b}^s$, leaving $\mathbf{a}_s$ and $\mathbf{b}^r$ unaffected, and it is related to the non-stiffness of the simplified model [20, 21, 23, 44].

- Assuming that "k_1" $\mathbf{b}^r$-refinements and "m_1" $\mathbf{a}_r$-refinements have already being made, an additional $\mathbf{b}^r$-refinement that improves the accuracy of $\mathbf{a}_s$ and $\mathbf{b}^r$ vectors is provided by the following relations:

$$\mathbf{b}^r(k_1+1,m_1) = \boldsymbol{\tau}_r^r(k_1,m_1)\left[\frac{d\mathbf{b}^r(k_1,m_1)}{dt} + \mathbf{b}^r(k_1,m_1)\mathbf{J}\right]$$

$$\mathbf{a}_r(k_1+1,m_1) = \mathbf{a}_r(k_1,m_1)$$

$$\mathbf{b}^s(k_1+1,m_1) = \mathbf{b}^s(k_1,m_1)$$

$$\mathbf{a}_s(k_1+1,m_1) = \left[\mathbf{I} - \mathbf{a}_r(k_1+1,m_1)\mathbf{b}^r(k_1+1,m_1)\right]\mathbf{a}_s(k_1,m_1)$$

where

$$\boldsymbol{\tau}_r^r(k_1,m_1) = (\boldsymbol{\lambda}_r^r(k_1,m_1))^{-1}$$

$$= \left[\left(\frac{d\mathbf{b}^r(k_1,m_1)}{dt} + \mathbf{b}^r(k_1,m_1)\mathbf{J}\right)\mathbf{a}_r(k_1+1,m_1)\right]^{-1}$$

- Assuming that "k_2" $\mathbf{b}^r$-refinements and "m_2" $\mathbf{a}_r$-refinements have already being made, an additional $\mathbf{a}_r$-refinement that improves the accuracy of $\mathbf{a}_r$ and $\mathbf{b}^s$ vectors is provided by the following relations:

$$\mathbf{a}_r(k_2,m_2+1) = \left[-\frac{d\mathbf{a}_r(k_2,m_2)}{dt} + \mathbf{J}\mathbf{a}_r(k_2,m_2)\right]\boldsymbol{\tau}_r^r(k_2,m_2)$$

$$\mathbf{b}^r(k_2,m_2+1) = \mathbf{b}^r(k_2,m_2)$$

$$\mathbf{b}^s(k_2,m_2+1) = \mathbf{b}^s(k_2,m_2)\left[\mathbf{I} - \mathbf{a}_r(k_2,m_2+1)\mathbf{b}^r(k_2,m_2+1)\right]$$

$$\mathbf{a}_s(k_2,m_2+1) = \mathbf{a}_s(k_2,m_2)$$

where

$$\boldsymbol{\tau}_r^r(k_2,m_2) = (\boldsymbol{\lambda}_r^r(k_2,m_2))^{-1}$$

$$= \left[\left(\frac{d\mathbf{b}^r(k_2,m_2)}{dt} + \mathbf{b}^r(k_2,m_2)\mathbf{J}\right)\mathbf{a}_r(k_2+1,m_2)\right]^{-1}$$

2.1 Implementation of the CSP refinements

The implementation of the CSP-refinements starts by assuming an initial guess for the basis vectors $\mathbf{a}_i$ and $\mathbf{b}^i$, $i = 1, \ldots, N$. If these basis vectors are constants, the time derivative terms are ignored in the first implementation of the refinements, which in the following will be referred as "Phase (1)". The time derivative terms will be retained in the following implementations of the refinements, which in the following will be referred as "Phase (2)". Since in the general case of a non linear system the time derivatives contribute to higher order accuracy, the "Phase (1)" of the CSP refinements involves only one set of $\mathbf{b}^r$ and $\mathbf{a}_r$-refinements. On the other hand, "Phase (2)" can involve more than one set of refinements [38]. The only limitation in this case is set by the increasing computational cost, as it will be shown explicitly next.

Differentiating Eq.(2.9) with respect to time, along a solution of a trajectory $\mathbf{y}(t)$, yields:

$$\frac{df^i}{dt} = \sum_{j=1}^{N} \lambda_j^i f^j \tag{2.11}$$

where i=1,..., N and

$$\boldsymbol{\lambda}_j^i \equiv \left(\frac{d\mathbf{b}^i}{dt} + \mathbf{b}^i \bullet \mathbf{J} \right) \bullet \mathbf{a}_j \tag{2.12}$$

where i,j = 1,..., N. In vector form Eq.(2.11) yields:

$$\frac{d}{dt} \begin{bmatrix} \mathbf{f}^r \\ \mathbf{f}^s \end{bmatrix} = \begin{bmatrix} \boldsymbol{\lambda}_r^r & \boldsymbol{\lambda}_s^r \\ \boldsymbol{\lambda}_r^s & \boldsymbol{\lambda}_s^s \end{bmatrix} \begin{bmatrix} \mathbf{f}^r \\ \mathbf{f}^s \end{bmatrix} \tag{2.13}$$

where r=1, ... , M and s=M+1, ... , N. The $\mathbf{b}^r$-refinements tend to reduce the order of $\boldsymbol{\lambda}_s^r$, while the $\mathbf{a}_r$-refinements tend to reduce the order of $\boldsymbol{\lambda}_r^s$. Evidently, these features result to (i) the decoupling of the fast time scales from the slow ones, when $\boldsymbol{\lambda}_s^r \to 0$ and (ii) the decoupling of the slow time scales from the fast ones, when $\boldsymbol{\lambda}_r^s \to 0$) [38].

2.1.1 Phase (1) of the *CSP* refinements

Consider the case where the first guess for the CSP vectors is the constant vectors $\mathbf{b}^r(0,0)$ and $\mathbf{a}_r(0,0)$, so:

$$\frac{d\mathbf{b}^r(0,0)}{dt} = 0, \qquad \frac{d\mathbf{a}_r(0,0)}{dt} = 0 \tag{2.14}$$

In this case, the CSP algorithm for the first $\mathbf{b}^r$-refinement yields:

$$\mathbf{b}^r(1,0) = \boldsymbol{\lambda}_r^r(0,0)\mathbf{b}^r(0,0)\mathbf{J}$$

$$\mathbf{a}_r(1,0) = \mathbf{a}_r(0,0)$$

$$\mathbf{b}^s(1,0) = \mathbf{b}^s(0,0)$$

$$\mathbf{a}_s(1,0) = [\mathbf{I} - \mathbf{a}_r(1,0)\mathbf{b}^r(1,0)]\mathbf{a}_s(0,0) = [\mathbf{I} - \mathbf{a}_r(0,0)\mathbf{b}^r(1,0)]\mathbf{a}_s(0,0)$$

where:

$$\boldsymbol{\lambda}_r^r(0,0) = \mathbf{b}^r(0,0)\mathbf{J}\mathbf{a}_r(0,0) \qquad\qquad \boldsymbol{\tau}_r^r(0,0) = [\boldsymbol{\lambda}_r^r(0,0)]^{-1}$$

The effect of the $\mathbf{b}^r$-refinement is to lower the norm of $\boldsymbol{\lambda}_s^r$ (where $(d\mathbf{b}^r(1,0)/dt) \bullet \mathbf{a}_s(1,0) = \mathbf{0}_s^r$):

$$\boldsymbol{\lambda}_s^r(1,0) = \mathbf{b}^r(1,0)\mathbf{J}\mathbf{a}_s(1,0) = \bigcirc(\epsilon\boldsymbol{\lambda}_s^r(0,0))$$

by an order of $\epsilon = |\tau_M/\tau_{M+1}| < 1$, making the fast modes "purer", by decoupling them from the slow modes, while the decoupling level of the slow time scales with the fast time scales is left unchanged:

$$\boldsymbol{\lambda}_r^s(1,0) = \mathbf{b}^s(1,0)\mathbf{J}\mathbf{a}_r(1,0) = \mathbf{b}^s(0,0)\mathbf{J}\mathbf{a}_r(0,0) = \boldsymbol{\lambda}_r^s(0,0)$$

Given the CSP vectors after one $\mathbf{b}^r$-refinement, the algorithm of the $\mathbf{a}_r$-refinement yields:

$$\mathbf{a}_r(1,1) = \mathbf{J}\mathbf{a}_r(0,0)\boldsymbol{\tau}_r^r(1,0)$$

$$\mathbf{b}^r(1,1) = \mathbf{b}^r(1,0)$$

$$\mathbf{a}_s(1,1) = \mathbf{a}_s(1,0)$$

$$\mathbf{b}^s(1,1) = \mathbf{b}^s(1,0)[\mathbf{I} - \mathbf{a}_r(1,1)\mathbf{b}^r(1,1)] = \mathbf{b}^s(0,0)[\mathbf{I} - \mathbf{a}_r(1,1)\mathbf{b}^r(1,0)]$$

where:

$$\boldsymbol{\lambda}_r^r(1,0) = \mathbf{b}^r(1,0)\mathbf{J}\mathbf{a}_r(0,0) \qquad\qquad \boldsymbol{\tau}_r^r(1,0) = [\boldsymbol{\lambda}_r^r(1,0)]^{-1}$$

The result of the $\mathbf{a}_r$-refinement is to lower the norm of $\boldsymbol{\lambda}_r^s$:

$$\boldsymbol{\lambda}_r^s(1,1) = \left[\frac{d\mathbf{b}^s(1,1)}{dt} + \mathbf{b}^s(1,1)\mathbf{J}\right]\mathbf{a}_r(1,1) = \bigcirc(\epsilon\boldsymbol{\lambda}_r^s(1,0)) = \bigcirc(\epsilon\boldsymbol{\lambda}_r^s(0,0))$$

by an order of $\epsilon = |\tau_M/\tau_{M+1}| < 1$, making the slow modes "purer", by decoupling them from the fast modes, while the decoupling level of the fast time scales with the slow time scales is left unchanged:

$$\boldsymbol{\lambda}_s^r(1,1) = \left[\frac{d\mathbf{b}^r(1,1)}{dt} + \mathbf{b}^r(1,1)\mathbf{J}\right]\mathbf{a}_s(1,1) = \left[\frac{d\mathbf{b}^r(1,0)}{dt} + \mathbf{b}^r(1,0)\mathbf{J}\right]\mathbf{a}_s(1,0)$$

$$= \boldsymbol{\lambda}_s^r(1,0) = \bigcirc(\epsilon\boldsymbol{\lambda}_s^r(0,0))$$

2.1.2 Phase (2) of the *CSP* refinements

The CSP vectors are now considered functions of the stated vector $\mathbf{y}$, so they are time dependent. The time derivatives of the basis vectors are taken into account, so that high-order terms are retained which result to a better decoupling between fast and slow modes [38]. Given the *CSP* basis vectors from Phase (1), one additional $\mathbf{b}^r$-refinement yields:

$$\mathbf{b}^r(2,1) = \boldsymbol{\tau}_r^r(1,1)\left[\frac{d\mathbf{b}^r(1,1)}{dt} + \mathbf{b}^r(1,1)\mathbf{J}\right] = \boldsymbol{\tau}_r^r(1,1)\left[\frac{d\mathbf{b}^r(1,0)}{dt} + \mathbf{b}^r(1,0)\mathbf{J}\right]$$

$$\mathbf{a}_r(2,1) = \mathbf{a}_r(1,1)$$

$$\mathbf{b}^s(2,1) = \mathbf{b}^s(1,1)$$

$$\mathbf{a}_s(2,1) = [\mathbf{I} - \mathbf{a}_r(2,1)\mathbf{b}^r(2,1)]\,\mathbf{a}_s(1,1) = [\mathbf{I} - \mathbf{a}_r(1,1)\mathbf{b}^r(2,1)]\,\mathbf{a}_s(1,0)$$

where:

$$\boldsymbol{\lambda}_r^r(1,1) = \left[\frac{d\mathbf{b}^r(1,1)}{dt} + \mathbf{b}^r(1,1)\mathbf{J}\right]\mathbf{a}_r(1,1) \qquad\qquad \boldsymbol{\tau}_r^r(1,1) = [\boldsymbol{\lambda}_r^r(1,1)]^{-1}$$

The result of the $\mathbf{b}^r$-refinement is to lower even more the norm of $\boldsymbol{\lambda}_s^r$:

$$\boldsymbol{\lambda}_s^r(2,1) = \left[\frac{d\mathbf{b}^r(2,1)}{dt} + \mathbf{b}^r(2,1)\mathbf{J}\right]\mathbf{a}_s(2,1) = \bigcirc(\epsilon\boldsymbol{\lambda}_s^r(1,1)) = \bigcirc(\epsilon\boldsymbol{\lambda}_s^r(1,0))$$

$$= \bigcirc(\epsilon^2\boldsymbol{\lambda}_s^r(0,0))$$

by an additional order of $\epsilon = |\tau_M/\tau_{M+1}| < 1$, making the fast time scales "purer", by decoupling them from the slow ones, while the decoupling level of the slow time scales with the fast ones is left unchanged:

$$\boldsymbol{\lambda}_r^s(2,1) = \left[\frac{d\mathbf{b}^s(2,1)}{dt} + \mathbf{b}^s(2,1)\mathbf{J}\right]\mathbf{a}_r(2,1) = \left[\frac{d\mathbf{b}^s(1,1)}{dt} + \mathbf{b}^s(1,1)\mathbf{J}\right]\mathbf{a}_r(1,1)$$

$$= \boldsymbol{\lambda}_r^s(1,1) = \bigcirc(\epsilon\boldsymbol{\lambda}_r^s(1,0)) = \bigcirc(\epsilon\boldsymbol{\lambda}_r^s(0,0))$$

Given the *CSP* basis vectors after the second $\mathbf{b}^r$-refinement, an additional $\mathbf{a}_r$-refinement yields:

$$\mathbf{a}_r(2,2) = \left[\frac{d\mathbf{a}_r(2,1)}{dt} + \mathbf{b}^r(2,1)\mathbf{J}\right]\boldsymbol{\tau}_r^r(2,1) = \left[\frac{d\mathbf{a}_r(1,1)}{dt} + \mathbf{J}\mathbf{a}_r(1,1)\right]\boldsymbol{\tau}_r^r(2,1)$$

$$\mathbf{b}^r(2,2) = \mathbf{b}^r(2,1)$$

$$\mathbf{a}_s(2,2) = \mathbf{a}_s(2,1)$$

$$\mathbf{b}^s(2,2) = \mathbf{b}^s(2,1)[\mathbf{I} - \mathbf{a}_r(2,2)\mathbf{b}^r(2,2)] = \mathbf{b}^s(1,1)[\mathbf{I} - \mathbf{a}_r(2,2)\mathbf{b}^r(2,1)]$$

where:

$$\boldsymbol{\lambda}_r^r(2,1) = \left[\frac{d\mathbf{b}^r(2,1)}{dt} + \mathbf{b}^r(2,1)\mathbf{J}\right]\mathbf{a}_r(2,1) \qquad\qquad \boldsymbol{\tau}_r^r(2,1) = [\boldsymbol{\lambda}_r^r(2,1)]^{-1}$$

The result of the second $\mathbf{a}_r$-refinement is to lower even more the norm of $\boldsymbol{\lambda}_r^s$:

$$\boldsymbol{\lambda}_s^r(2,2) = \left[\frac{d\mathbf{b}^s(2,2)}{dt} + \mathbf{b}^s(2,2)\mathbf{J}\right]\mathbf{a}_r(2,2) = \bigcirc(\epsilon\boldsymbol{\lambda}_r^s(2,1))$$

$$= \bigcirc(\epsilon^2\boldsymbol{\lambda}_r^s(1,0)) = \bigcirc(\epsilon^2\boldsymbol{\lambda}_r^s(0,0))$$

by an additional order of $\epsilon = |\tau_M/\tau_{M+1}| < 1$, making the slow modes "purer", by decoupling them from the fast modes, while the decoupling of the fast modes from the slow ones is left unchanged:

$$\boldsymbol{\lambda}_s^r(2,2) = \left[\frac{d\mathbf{b}^r(2,2)}{dt} + \mathbf{b}^r(2,2)\mathbf{J}\right]\mathbf{a}_s(2,2) = \left[\frac{d\mathbf{b}^r(2,1)}{dt} + \mathbf{b}^r(2,1)\mathbf{J}\right]\mathbf{a}_s(2,1)$$

$$= \boldsymbol{\lambda}_s^r(2,1) = \bigcirc(\epsilon\boldsymbol{\lambda}_s^r(1,1)) = \bigcirc(\epsilon\boldsymbol{\lambda}_s^r(1,0)) = \bigcirc(\epsilon^2\boldsymbol{\lambda}_s^r(0,0))$$

2.1.3 Time derivatives of the Jacobian

In order to calculate the *CSP* basis vectors in Phase (2), a number of time derivatives of the CSP vectors must be computed [38]. The main expressions used for this purpose are:

$$\frac{d\mathbf{b}^r(1,1)}{dt} = \frac{d\mathbf{b}^r(1,0)}{dt} = \boldsymbol{\tau}_r^r(0,0)\mathbf{b}^r(0,0)\frac{d\mathbf{J}}{dt}\left[\mathbf{I} - \mathbf{a}_r(0,0)\mathbf{b}^r(1,0)\right] \tag{2.15}$$

$$\frac{d\mathbf{a}_r(2,1)}{dt} = \frac{d\mathbf{a}_r(1,1)}{dt} = [\mathbf{I} - \mathbf{a}_r(1,1)\mathbf{b}^r(1,0)]\frac{d\mathbf{J}}{dt}\mathbf{a}_r(0,0)\boldsymbol{\tau}_r^r(1,0)$$
$$- \mathbf{a}_r(1,1)\frac{d\mathbf{b}^r(1,0)}{dt}\mathbf{a}_r(1,1) \tag{2.16}$$

$$\frac{d\mathbf{b}^r(2,1)}{dt} = \boldsymbol{\tau}_r^r(1,1)\left[\frac{d\mathbf{b}^r(1,0)}{dt}\mathbf{J} + \mathbf{b}^r(1,0)\frac{d\mathbf{J}}{dt} + \frac{d^2\mathbf{b}^r(1,0)}{dt^2}\right][\mathbf{I} - \mathbf{a}_r(1,1)\mathbf{b}^r(2,1)]$$
$$- \mathbf{b}^r(2,1)\frac{d\mathbf{a}_r(1,1)}{dt}\mathbf{b}^r(2,1) \tag{2.17}$$

where

$$\frac{d^2\mathbf{b}^r(1,0)}{dt^2} = \left[\frac{d\boldsymbol{\tau}_r^r(0,0)}{dt}\mathbf{b}^r(0,0)\frac{d\mathbf{J}}{dt} + \boldsymbol{\tau}_r^r(0,0)\mathbf{b}^r(0,0)\frac{d^2\mathbf{J}}{dt}\right][\mathbf{I} - \mathbf{a}_r(0,0)\mathbf{a}^r(1,0)]$$
$$- \boldsymbol{\tau}_r^r(0,0)\mathbf{b}^r(0,0)\frac{d\mathbf{J}}{dt}\mathbf{a}_r(0,0)\frac{d\mathbf{b}^r(1,0)}{dt} \tag{2.18}$$

The time derivatives involve the evaluation of the time rate change of the Jacobian matrix $d\mathbf{J}/dt$ and the high order rates $d^2\mathbf{J}/dt^2$ as well:

$$\frac{d\mathbf{J}}{dt} = \sum_{i=1,N_s} \frac{\partial \mathbf{J}}{\partial y^i} \frac{d\mathbf{y}^i}{dt} = \sum_{i=1,N_s} \frac{\partial \mathbf{J}}{\partial y^i} \mathbf{g}^i \tag{2.19}$$

$$\frac{d^2\mathbf{J}}{dt^2} = \sum_{i,j=1,N_s} \left[\frac{\partial^2 \mathbf{J}}{\partial y^i \partial y^j} \mathbf{g}^i + \frac{\partial \mathbf{J}}{\partial y^i} \mathbf{J} \right] \mathbf{g}^j \tag{2.20}$$

The fact that the time derivatives of the Jacobian are required for the description of the *SIM* and of the slow system only in Phase (2) suggests that the curvature of the *SIM* contributes in high order accuracy terms only [38].

2.2 The Criteria to identify the M number of the exhausted modes

The number M of the fast exhausted time scales of the system and the dimensions of the *SIM* $N - M$, might change as a the solution evolves with time. The identification of the number of the exhausted time scales depends on the order of accuracy that is sought. Here, the criteria for leading (first) and second order accuracy will be stated. The measure for the order of accuracy will be the fast/slow time scale ratio $\epsilon = \tau_M / \tau_{M+1}$.

2.2.1 First order accuracy

Demanding leading order accuracy, the criterion for declaring the M fast time scales exhausted is:

$$\tau_{M+1} \left| \mathbf{a}_r(1,1) \mathbf{f}^r(1,1) \right| \; < \; \frac{\tau_M}{\tau_{M+1}} |\mathbf{y}| + \mathbf{AbsErr} \tag{2.21}$$

where $\mathbf{a}^r(1,1)$ is the $(N \times M)$-dim. matrix containing the M fast *CSP* basis vectors (see Eq. (2.4)) computed after performing one $\mathbf{b}^r$- and one $\mathbf{a}_r$-refinements and $\mathbf{f}^r(1,1)$ (see Eq. (2.9)) is the M-dim. vector with the M amplitudes of the M fast *CSP* modes computed after performing one $\mathbf{b}^r$- and one $\mathbf{a}_r$-refinements. The first term in the RHS of Eq. (2.21) indicates the relative error allowed when integrating the slow system, while the second term denotes the equivalent absolute error. The results that will be reported next were computed by setting $\mathbf{AbsErr}^i = 10^{-16}$ for all $i = 1, \ldots, N$.

2.2.2 Second order accuracy

Seeking second order accuracy, the criterion for declaring the M fast time scales exhausted is:

$$\tau_{M+1} \left| \mathbf{a}_r(2,1) \mathbf{f}^r(2,1) \right| \; < \; \left(\frac{\tau_M}{\tau_{M+1}} \right)^2 |\mathbf{y}| + \mathbf{AbsErr} \tag{2.22}$$

where the $\mathbf{a}^r(2,1)$ $(N \times M)$-dim. matrix contains the M fast *CSP* basis vectors (see Eq. (2.4)) computed after performing two $\mathbf{b}^r$- and one $\mathbf{a}_r$-refinements and $\mathbf{f}^r(2,1)$ (see Eq. (2.9)) is the M-dim. vector with the M amplitudes of the M fast *CSP* modes computed after performing two $\mathbf{b}^r$- and one $\mathbf{a}_r$-refinements. As when seeking leading order accuracy, the first term in the RHS of Eq. (2.22) indicates the relative error allowed when integrating the slow system, while the second term denotes the equivalent absolute error. The results that will be reported next were computed by setting $\mathbf{AbsErr}^i = 10^{-16}$ for all $i = 1, \ldots, N$.

2.3 The CSP diagnostic tools

CSP allows for the development of a number of computational tools by which the meaningful physical understanding for the evolution of the system under examination can be acquired.

It is assumed that the vector field $\mathbf{g}(\mathbf{y})$ represents $2K$ physical processes that are represented by the products $\mathbf{S}_k R^k$ $(k = 1, ..., 2K)$:

$$\mathbf{g}(\mathbf{y}) \;=\; \mathbf{S}_1 R^1(\mathbf{y}) + \mathbf{S}_2 R^2(\mathbf{y}) + \ldots \mathbf{S}_{2K} R^{2K}(\mathbf{y}) \tag{2.23}$$

where $\mathbf{S}_k$ is the constant stoichiometric vector of the k-th process and $R^k(\mathbf{y})$ is the corresponding rate. Therefore, the amplitude of the i-th CSP mode f^i $(i = 1, \ldots, N$; see Eq. (2.6)), can be expressed as:

$$f^i \;=\; f_1^i + ... + f_{2K}^i \tag{2.24}$$

where $f_k^i(\mathbf{y}) = (\mathbf{b}^i \bullet \mathbf{S}_k) R^k(\mathbf{y})$. When f^m represents an exhausted mode $(m = 1, \ldots, M$; see Eq. (2.9)), Eq. (2.24) yields:

$$f^m \;=\; f_1^m + ... + f_{2K}^m \approx 0 \tag{2.25}$$

2.3.1 The CSP Pointer

The variables that are affected the most by the m-th fast time scale and exhibit a significant influence on the terms participating in the occurring cancelations in the vanishing amplitude of the m-th mode, see Eq. (2.25), can be identified by the the *CSP Pointer* for the m-th mode:

$$\mathbf{D}^m = diag[\mathbf{a}_m \mathbf{b}^m] = [a_m^1 b_1^m, ..., a_m^N b_N^m]^T \tag{2.26}$$

where due to the orthogonality $\mathbf{b}^m \cdot \mathbf{a}_m = 1$, it follows that $a_m^1 b_1^m + ... + a_m^N b_N^m = 1$, $(m = 1, \ldots, M)$ [9, 20, 23]. A value of $a_m^j b_j^m$ $(j = 1, ..., N)$ close to unity denotes the association of the j-th variable with the m-th *CSP mode* $\mathbf{a}_m f^m$ and the related time scale τ_m.

2.3.2 The Participation Index

Eq.(2.25) indicates that the decay to negligible values of the exhausted fast amplitudes is the result of equilibrations emerging among various components in the model. These components are identified with the use of the *Participation Index*:

$$P_k^m = \frac{f_k^m(\mathbf{y})}{\sum_{j=1}^{2K} |f_j^m(\mathbf{y})|} \tag{2.27}$$

where m denotes the fast *CSP* mode $(m = 1, \ldots, M)$, k denotes the k-th component $(k = 1, ..., 2K)$ and by definition $|P_1^m| + ... + |P_k^m| = 1$ [9, 20, 23]. Since only exchausted modes are considered, for which $f^m \approx 0$, the following relation also holds: $P_1^m + ... + P_k^m \approx 0$. As a result, a relatively large value of P_k^m indicates a large contribution of the k-th process to the constraint developed along the m-th *CSP* basis vector $\mathbf{a}_m$, imposed by the m-th fast time scale, when becomes exhausted.

2.3.3 The Importance Index

The flow on the *SIM* is governed by the slow system in Eq. (2.10):

$$\frac{d\mathbf{y}}{dt} \approx \mathbf{a}_s \mathbf{f}^s = \mathbf{g}_{slow}$$

The contribution of the k-th process to the evolution on the *SIM* of the n-th variable in $\mathbf{y}$, according to the slow system, can be evaluated with the *CSP Importance Index*, which is defined as follows. Each element of $\mathbf{g}_{slow}(\mathbf{y})$ can be expressed in terms of the $2K$ processes as:

$$g^n_{slow}(\mathbf{y}) = g^{n,1}_{slow}(\mathbf{y}) + g^{n,2}_{slow}(\mathbf{y}) + ... + g^{n,2K}_{slow}(\mathbf{y}) \tag{2.28}$$

where $g^{n,2K}_{slow}(\mathbf{y}) = \sum_{j=M+1}^{N} a^n_j (\mathbf{b}^j \bullet \mathbf{S}_k) R^k(\mathbf{y})$, $(k = 1, ..., 2K)$ and a^n_j denoted the n-th element of the column vector $\mathbf{a}_j$ $(j = M+1, \ldots, N)$ in $\mathbf{a}_s$; see Eq.(2.5). The Importance Index is defined as:

$$I^n_k = \frac{g^{n,k}_{slow}(\mathbf{y})}{\sum_{j=1}^{2K} |g^{n,j}_{slow}(\mathbf{y})|} \tag{2.29}$$

where by definition $|I^n_1| + |I^n_2| + ... + |I^n_{2K}| = 1$ [9, 20]. A relatively large value of $|I^n_k|$ indicates that the k-th process provides a significant contribution to the evolution of y^n on the *SIM*, while a relatively small value of $|I^n_k|$ indicates a negligible contribution.

2.3.4 The Eigenvalue Participation Index

In general, all processes represented in the vector field $\mathbf{g}(\mathbf{y})$, see Eq. (2.23), contribute to the emergence of the M-fast dissipative time scales. The exact contribution of each process can be identified by the *Eigenvalue Participation Index (EPI)*, which provides the contibution of the k-th process to the development of the m-th eigenvalue λ_m. For a real eigenvalue λ_m it holds that:

$$\lambda_m = \mathbf{q}^m \mathbf{J} \mathbf{p}_m \tag{2.30}$$

where $\mathbf{q}_m$ and $\mathbf{p}_m$ are the corresponding left (row) and right (column) eigenvectors of the Jacobian $\mathbf{J}$. Substituting from Eq. (2.23) yields the following partition of the eigenvalue λ_m with respect to the $2K$ processes:

$$\lambda_m = \lambda^1_m + \lambda^2_m + ... + \lambda^{2K}_m \tag{2.31}$$

where

$$\lambda^k_m = \mathbf{q}^m \mathbf{S}_k \nabla R^k \mathbf{p}_m, \quad (k = 1, ..., 2K) \tag{2.32}$$

The EPI is defined as:

$$\Lambda^m_k = \frac{\lambda^k_m}{\sum_{j=1}^{2K} |\lambda^j_m|} \tag{2.33}$$

By definition $|\Lambda^n_1| + |\Lambda^n_2| + ... + |\Lambda^n_{2K}| = 1$ and the value of Λ^n_k provides a measure of the influence of the k-th process to the value of the n-th eigenvalue λ_n. [8, 10] Clearly, reactions whose rates are

constants cannot contibute to the generation of λ_n. Negative values of Λ_k^n indicate a trend to of the k-th process to move the n-th *CSP* mode towards equilibrium, i.e., $f^n(\mathbf{y}) \to 0$. These processes will be called dissipative ones. On the other hand, positive values of Λ_k^n indicate a trend away from equilibrium. Naturally, such processes will be declared as explosive ones. Regarding the exhausted time scales $\tau_m (m = 1, ..., M)$, in which the dissipative processes dominate, a non-negligible negative Λ_k^m indicates that the rate of the k-th process will act appropriately in order to restore, within a period of $O(\tau_m)$, the equilibration denoted by the m-th *CSP* mode $f^m(\mathbf{y}) \approx 0$. A positive Λ_k^m will oppose such action.

Chapter 3

The Wnt/β-catenin signaling pathway

Wnt is a protein ligand inside the extracellular space and when it is activated it binds to cell receptors on the surface of the cell and triggers the signaling process. The main protein that relates to the *Wnt* signaling process is thought to be *β-catenin*. Therefore, the identification of means to control the concentration of *β-catenin* is of great importance. The different way of bindings (i.e., different combinations of *Wnt* ligands and receptors at the cell surface) defines different *Wnt* pathways [27]. One of the most prominent bindings is the *Canonical Wnt* pathway.

In this study the model introduced by *Lee et al.* about the *Canonical Wnt* pathway will be analyzed. This pathway incorporates two states: (i) the reference state, where there is no *Wnt* signaling and the (ii) stimulated state, where the *Wnt* ligand binds to the cell receptors and trigers the signaling. As it is shown in Fig. 3.1, the basic functions between the proteins and protein complexes that take place in these two states are:

Reference state:

- In the absence of *Wnt* signaling, *β-catenin* in the cytosol binds to *Axin*, *APC*, *GSK3* and $CK1_a$, forming a complex (*destruction complex*) [11, 26, 33],
- inside this complex, *β-catenin* is phosphorylated by *GSK3* and $CK1_a$ [26],
- phosphorylated *β-catenin* is then leaded to ubiquitination and degradation by the proteasome, so that it does not enter the nucleus of the cell [30],
- in the nucleus the transcription factors of *(TCF/LEF)* complex bind to transcriptional receptors so that the activation of *Wnt* target genes is supressed [5].

Stimulated state:

- The *Wnt-protein ligand* binds in the surface of the cell to a *(Frizzled/LRP5)* receptor complex, which enables the *Dishvelled (Dsh)* and *Axin* proteins in the cytosol [2, 13],
- this signaling leads the *destruction complex* to accumulate *β-catenin*, so that *β-catenin* gets inside the nucleus [3],
- in the nucleus *β-catenin* binds to the *(TCF/LEF)* complex and this leads to the transcription of the *Wnt* targeted genes [3].

The function of the various proteins and protein complexes, shown in Fig. 3.1, can be briefly explained as follows. *β-catenin* is a dual function protein that regulates the coordination of cell-cell adhesion and gene transcription, as seen in the *Wnt* pathway. *Adenomatous Polyposis Coli* (APC) is a negative regulator protein that controls *β-catenin* concentrations, *Glycogen Synthase Kinase-3β* ($GSK3\beta$) is a *protein kinase* that mediates the addition of phosphate molecules onto serine and threonine amino acid residues, *Casein Kinase 1a* ($CK1_a$) is a protein kinase which is serine and threonine selective enzyme. *Axin* is a protein that in humans is encoded by the $AXIN1$ gene. The *(TCF/LEF)* family is a group of transcription factors which bind to *DNA* through a high mobility group domain.

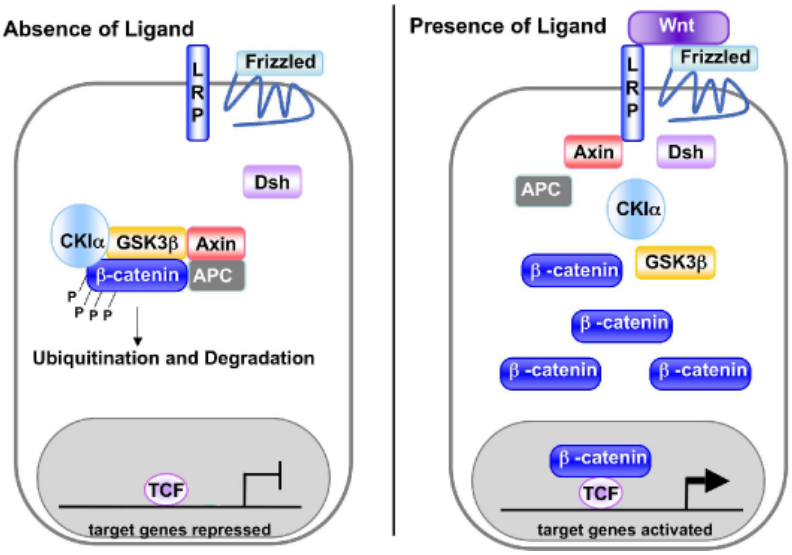

Figure 3.1: left; the absence of *Wnt* ligand let the destruction complex *(CKIα, GSK3β, APC, Axin)* to hyperphosphorylate *β-catenin* which then is a target for ubiqitination and degradation by the proteosome. right; the binding of *Wnt* ligand to a *Frizzled, LRP-5/6* receptor complex leads to the stabilization of the hypophosphorylated *β-catenin* which then interacts with *TCF/LEF* proteins in the nucleus to activate transcription; *CKIα* is a casein kinase that was found to play a role in the *Wnt* model [31], in the model by *Lee et al.* that we study in this work *CKIα* and *LRP-5/6* are not taken into account [25]; this figure was originally created by [6]

3.1 The Wnt/β-catenin signaling model

The *Wnt* model introduced by *Lee et al.*, as it is shown in Fig.(3.2), introduced results that (i) reproduced the *Wnt* pathway experimental results [24, 25, 34] in the *reference state* and (ii) were used to predict the behavior of the system during the *stimulated state* as well [25].

The *Wnt* model, which is depicted in Fig. 3.2, includes 17 reactions (steps) and 15 proteins and protein complexes (species). Except reactions 6, 7, 8, 16 and 17, all other reactions are uni-directional. The most important features of this model are (i) the participation of β-*catenin* in core complexes and (ii) the phosphorylation and destruction of β-*catenin*. Except from β-*catenin*, these complexes include the proteins *GSK3*β, *APC* and *Axin*. The steps that assemble or decompose these complexes are the forward reactions 4-10. Among the various steps of the pathway are: (i) the synthesis of *Axin* and of β-*catenin* (reactions 14 and 12), (ii) the degradation of *Axin* (reaction 15), (iii) the *Axin*-dependent degradation of β-*catenin* (reaction 13), and (iv) the steps participating in the Destruction Core Cycle in order for phosphorylated β-*catenin* to be degraded (reactions 8, 9, 10, 11) [25].

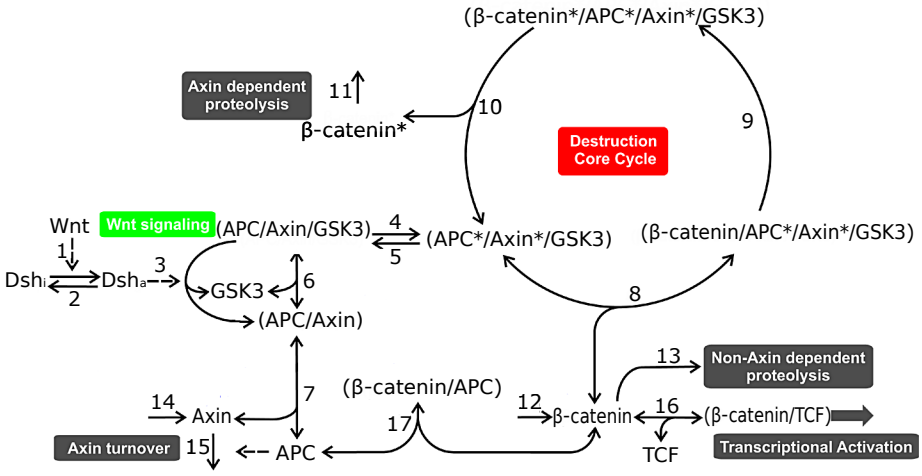

Figure 3.2: The 17 reaction scheme of the Wnt pathway by *Lee et al.*; single arrows characterize one way reactions, double arrows denote binding equilibria, broken arrows represent: *Dsh* activation by Wnt-stimulation, Dsh-mediated initiation of the release of *GSK3*β from the destruction complex and degradation of *Axin* through *APC* mediation (arrows 1,3,15); asterisks denote phosphorylation.

In the reference state where there is no *Wnt* signaling $Wnt = 0$. As suggested by Fig. 3.2, *Dsh* is inactive and it does not affect the degradation complex, so that the concentration of β-*catenin* is expected to stay low due to the continuous phosphorylation and degradation. In the stimulated state $Wnt = 1$, so that the concentration of β-*catenin* is expected to be higher, producing larger amounts of (β-*catenin/TCF*). As a result the concentrations of β-*catenin** and *TCF* are expected to be lower. The concentration of *Axin* is constant whether we have the reference or the stimulated state because *Axin* synthesis and degradation are independent of the *Wnt*-stimulation. These estimates will be validated in the following sections, when numerical results will be presented.

All the reaction rates of the model are listed in Table 3.1. The rate equations presented in Table 3.1 are functions of mass action rate constants k_j for $j = 1, ..., 17$ and concentrations X_i for $i = 1, ..., 15$. The values of the rate constants and of the initial conditions for the concentrations employed here are listed in Table 3.2. The initial conditions of the concentrations for Dsh_i (X_1), APC (X_7), TCF (X_{13}), GSK3 (X_5), *Axin* (X_{12}) and *β-catenin* (X_{11}), see Table 3.2, were determined experimentaly by *Lee et al.* using Western blot analysis (Western blot analysis is a widely used analytical technique used to detect specific proteins in a sample of tissue homogenate or extract) [25]. The initial value for the concentration of *β-catenin** (X_{10}) was estimated, because it couldn't be specified by experiment [25]. The initial conditions for the remaining concentrations were specified (i) by assuming initial absence of *(APC*/Axin*/GSK3)* (X_3), *(APC/Axin/GSK3)* (X_4), *(β-catenin/APC*/Axin*/GSK3)* (X_8) and *(β-catenin*/APC*/Axin*/GSK3)* (X_9) and (ii) by employing the conservation laws for Dsh_a (X_2), *(APC/Axin)* (X_6) and *(β-catenin/APC)* (X_{15}).

The dissociation constants $K_i = k_{-i}/k_{+i}$ for $i = 7, 8, 16, 17$ were estimated using experimental results. The rate constants $k_4, k_5, k_{-6}, k_{+6}, k_9 - k_{15}$ were calculated using dissociation constants data and conservation laws, along with steady state concentrations [25]. The values of parameters that remain unknown were chosen so that the *β-catenin* degradation rate matched the experimental results [27].

The model has 4 conservation equations, depicted in Table 3.3. The time derivatives of the sums participating in the conservation equations equal to zero. The conserved quantities are the total concetrations of *Dsh*, *GSK3*, *APC* and *TCF* and their values are given in Table 3.3.

Lee et al. assumed that the reversible binding steps involving *APC* (step 7), *Axin* (step 8), *TCF* (step 16) and *β-catenin* (step 17) are very fast and equilibrate with their forward steps [25]. As a result, the *Partial Equilibrium* approximation holds for reactions 7, 8, 16 and 17, so that $V_{7f} - V_{7b} \approx 0$, $V_{8f} - V_{8b} \approx 0$, $V_{16f} - V_{16} \approx 0$ and $V_{17f} - V_{17b} \approx 0$.

Implementation of these four approximation yields a 15 dimensional ODE system, in which the rates of the reactions in partial equilibrium (V_7, V_8, V_{16} and V_{17}) are substituted by the equilibrium relations that involve the remaining rates $V_4 - V_6$, V_9 and $V_{12} - V_{15}$. A complete list of the modified ODE system is presented in Table 3.4. The differential equations that are altered with the implementation of the four *Partial Equilibrium* approximations are those involving the rate of change of $\dot{X}_3$, $\dot{X}_6$, $\dot{X}_7$, $\dot{X}_8$, $\dot{X}_{11}$-$\dot{X}_{15}$. The use of C_m for $m = 1, ..., 90$ notation is due to the complexity of these functions.

The concentration of the *Wnt-ligand* is denoted by W. In the absence of Wnt signaling ($W = 0$) the rate of the first reaction is zero ($V_1 = 0$), so that the rate of change equations for X_1 and X_2 reduce to $\dot{X}_1 = V_2$ and $\dot{X}_2 = -V_2$. Given the initial conditions $X_1(t = 0) = 100$ and $X_2(t = 0) = 0$, $V_1(t) = V_2(t) = V_3(t) = 0$, so that and $\dot{X}_1 = \dot{X}_2 = 0$.

Table 3.1: The reactions rates V_k, $(k = 1, ..., 17)$ are functions of the concentrations of the proteins and protein complexes X_i, $(i = 1, ..., 15)$ in the model. Binding and dissociation processes (reactions 6, 7, 8, 16 and 17) are bidirectional. Synthesis processes (12 and 14) have constant rates. In V_1, W=0 or 1 in the reference or stimulated state, respectively.

$V_1 = k_1 * W * X_1$	activation of *Dsh* by *Wnt*
$V_2 = k_2 * X_2$	deactivation of *Dsh*
$V_3 = k_3 * X_2 * X_4$	dissociation of *GSK3* from the destruction complex
$V_4 = k_4 * X_4$	phosphorylation of *Axin* and *APC*
$V_5 = k_5 * X_3$	dephosphorylation of *Axin* and *APC*
$V_6 = k_6^+ * X_5 * X_6 - k_6^- * X_4$	binding of *GSK3* to the *(APC/Axin)* complex
	and dissociation of *GSK3* from the destruction complex
$V_7 = k_7^+ * X_7 * X_{12} - k_7^- * X_6$	binding of *APC* to *Axin*
	and dissociation of *APC* from the *(APC/Axin)* complex
$V_8 = k_8^+ * X_3 * X_{11} - k_8^- * X_8$	binding of *β-catenin* to the destruction complex
	and dissociation of *β-catenin* from the destruction complex
$V_9 = k_9 * X_8$	phosphorylation of *β-catenin*
$V_{10} = k_{10} * X_9$	dissociation of phosphorylated *β-catenin*
$V_{11} = k_{11} * X_{10}$	degradation of phosphorylated *β-catenin*
$V_{12} = k_{12}$	synthesis of *β-catenin*
$V_{13} = k_{13} * X_{11}$	degradation of *β-catenin*
$V_{14} = k_{14}$	synthesis of *Axin*
$V_{15} = k_{15} * X_{12}$	degradation of *Axin*
$V_{16} = k_{16}^+ * X_{11} * X_{13} - k_{16}^- * X_{14}$	binding of *TCF* to *β-catenin*
	and dissociation of *TCF* from (*β-catenin/TCF)*
$V_{17} = k_{17}^+ * X_7 * X_{11} - k_{17}^- * X_{15}$	binding of *APC* to *β-catenin*
	and dissociation of *APC* from *(β-catenin/APC)*

Table 3.2: (a) The initial concentrations for the variables in the model, taken from *Lee et al.* [25] (b) The values of the rate constants k_i in the model; K_i are the dissociation constants; k_{12} and k_{14} are the synthesis fluxes (constants); kinetic parameters marked with (#) play a role only in the stimulated state. Notation is adapted from *Lee et al.*; nM stands for "nano Mol" and min stands for "minutes".

(a)

Symbol	Description	values
X_1	Dsh_i	100 nM
X_2	Dsh_a	0 nM
X_3	*(APC*/Axin*/GSK3)*	0 nM
X_4	*(APC/Axin/GSK3)*	0 nM
X_5	*GSK3*	50.0 nM
X_6	*(APC/Axin)*	0.039 nM
X_7	*APC*	100 nM
X_8	*(β-catenin/APC*/Axin*/GSK3)*	0 nM
X_9	*(β-catenin*/APC*/Axin*/GSK3)*	0 nM
X_{10}	*β-catenin**	1.00 nM
X_{11}	*β-catenin*	35.0 nM
X_{12}	*Axin*	0.02 nM
X_{13}	*TCF*	6.92 nM
X_{14}	*(β-catenin/TCF)*	8.07 nM
X_{15}	*(β-catenin/APC)*	2.83 nM

(b)

Symbol	values
$k_1(\#)$	0.182 min^{-1}
$k_2(\#)$	$1.82 \cdot 10^{-2}$ min^{-1}
$k_3(\#)$	$5.00 \cdot 10^{-2}$ $nM^{-1}min^{-1}$
k_4	0.264 min^{-1}
k_5	0.133 min^{-1}
k_6	$9.09 \cdot 10^{-2}$ $nM^{-1}min^{-1}$
k_{-6}	0.909 min^{-1}
K_7	50 nM
K_8	120 nM
k_9	206 min^{-1}
k_{10}	206 min^{-1}
k_{11}	0.417 min^{-1}
k_{12}	0.423 nM min^{-1}
k_{13}	$2.57 \cdot 10^{-4}$ min^{-1}
k_{14}	$8.22 \cdot 10^{-5}$ nM min^{-1}
k_{15}	0.167 min^{-1}
K_{16}	30 nM
K_{17}	1200 nM

Table 3.3: The existing conservation equations. X_i, $(i = 1, ..., 15)$ are the concentrations of proteins and protein complexes in the model. Concentrations marked with ^{o} are total (constants). Notation as in *Lee et al.* [25]

$X_1 + X_2 = Dsh^o = 100$ nM
$X_3 + X_4 + X_5 + X_8 + X_9 = GSK3^o = 50$ nM
$X_3 + X_4 + X_6 + X_7 + X_8 + X_9 + X_{15} = APC^o = 100$ nM
$X_{13} + X_{14} = TCF^o = 15$ nM

Table 3.4: The system of differential equations governing the temporal evolution of the concentrations of proteins and protein complexes, assuming that rates V_7, V_8, V_{16} and V_{17} are in Partial Equilibrium (left); correspondence of X_i, $(i = 1, ..., 15)$ to protein and protein complexes (right); C_m, $(m = 1, ..., 90)$ are functions of concentrations X_i and of the dissociation constants K_7, K_8, K_{16} and K_{17}. Notation as in *Lee et al.* [25].

$\dot{X}_1 = -V_1 + V_2$	Dsh_i
$\dot{X}_2 = V_1 - V_2$	Dsh_a
$\dot{X}_3 = \sum_{i=3}^{6} C_{4-i}V_i + C_5V_9 + C_6V_{10} + \sum_{i=12}^{15} C_{i-5}V_i$	(APC*/Axin*/GSK3)
$\dot{X}_4 = -V_3 - V_4 + V_5 + V_6$	(APC/Axin/GSK3)
$\dot{X}_5 = V_3 - V_6$	GSK3
$\dot{X}_6 = \sum_{i=3}^{6} C_{8+i}V_i + C_{15}V_9 + C_{16}V_{10} + \sum_{i=12}^{15} C_{i+5}V_i$	(APC/Axin)
$\dot{X}_7 = \sum_{i=3}^{6} C_{18+i}V_i + C_{25}V_9 + C_{26}V_{10} + \sum_{i=12}^{15} C_{i+15}V_i$	APC
$\dot{X}_8 = \sum_{i=3}^{6} C_{28+i}V_i + C_{35}V_9 + C_{36}V_{10} + \sum_{i=12}^{15} C_{i+25}V_i$	(β-catenin/APC*/Axin*/GSK3)
$\dot{X}_9 = V_9 - V_{10}$	(β-catenin*/APC*/Axin*/GSK3)
$\dot{X}_{10} = V_{10} - V_{11}$	β-catenin*
$\dot{X}_{11} = \sum_{i=3}^{6} C_{38+i}V_i + C_{45}V_9 + C_{46}V_{10} + \sum_{i=12}^{15} C_{i+35}V_i$	β-catenin
$\dot{X}_{12} = \sum_{i=3}^{6} C_{48+i}V_i + C_{55}V_9 + C_{56}V_{10} + \sum_{i=12}^{15} C_{i+45}V_i$	Axin
$\dot{X}_{13} = \sum_{i=3}^{6} C_{58+i}V_i + C_{65}V_9 + C_{66}V_{10} + \sum_{i=12}^{15} C_{i+55}V_i$	TCF
$\dot{X}_{14} = \sum_{i=3}^{6} C_{68+i}V_i + C_{75}V_9 + C_{76}V_{10} + \sum_{i=12}^{15} C_{i+65}V_i$	(β-catenin/TCF)
$\dot{X}_{15} = \sum_{i=3}^{6} C_{78+i}V_i + C_{85}V_9 + C_{86}V_{10} + \sum_{i=12}^{15} C_{i+75}V_i$	(β-catenin/APC)

3.2 The dynamics of the *Wnt* model

The modified *Wnt* model presented in Table 3.4 was integrated for the reference and stimulated states and the related two solutions are presented in Fig. (3.3). In the reference state, shown at the top of Fig. (3.3), *Dsh* is inactive and the concentrations of Dsh_i and Dsh_a stay constant, $X_1 = 100$ and $X_2 = 0$ respectively. As explained in Chapter 3.1, the inactivation of *Dsh* is the reason for the lower values of the concentration of *β-catenin* (X_{11}), relative to those in the stimulated state, due to continuous phosphorylation and degradation. In the stimulated state the concentration of *β-catenin** (X_{10}) decreases from 1 nM (reference state) to 0.92 nM (stimulated state), shown in Fig. (3.3) by the magenta line. The concentration of the *(β-catenin/TCF)* (X_{14}) increases in the stimulated state from 6.83 nM (reference state) to 12.5 nM (stimulated state), shown in Fig. (3.3) by the dark tirquaz line. The increase in the stimulated state of the concentration of *β-catenin* (X_{11}) changes the concentration of (*β-catenin/APC*) (X_{15}) from 2.05 nM in the reference state to 11.3 nM in the stimulated state, shown in Fig. (3.3) by the green line. The concentration of *Axin* (X_{12}) is constant due to the rate of *Axin* synthesis ($V_{14} = k_{14}$), shown in Fig. (3.3) by the violet line.

The modified *Wnt* model which is analyzed here was constructed by applying the *PE* approximation for 4 reactions that were included in the full model of *Lee et al.* [25]. Therefore, the related 4 time scales of the original *Wnt* model are considered exhausted. Given the 4 conservation laws stated in Table 3.3 and the 4 *PE* approximations, the solution of the modified 15-dim. *Wnt* model evolves in a 7-dim. subspace of the state space.

The 7 bounded time scales of the modified *Wnt* model are displayed in Fig.(3.4), for the reference and stimulated state. The first 6 time scales are of dissipative character throughout the computational domain. The time scale τ_7 is of explosive character in the period ($0 < t < 0.63\ min$) in the reference state and ($0 < t < 0.54\ min$) in the stimulated, obtaining a dissipative character after these periods. It is observed that in both cases significant gaps develop among the time scales of the system, so that the multi-scale character of the model is verified. The basic difference between the two states relates to τ_5 (yellow line), which becomes faster in the simulated state by an $\bigcirc(10)$ relative to the reference state.

Using the kinetic parameters and the initial conditions displayed in Table 3.2, the modified *Wnt* model in Table 3.4 will be analyzed by employing *CSP* analysis. The use of the *CSP* algorithm is validated by the time scale separations that develop.

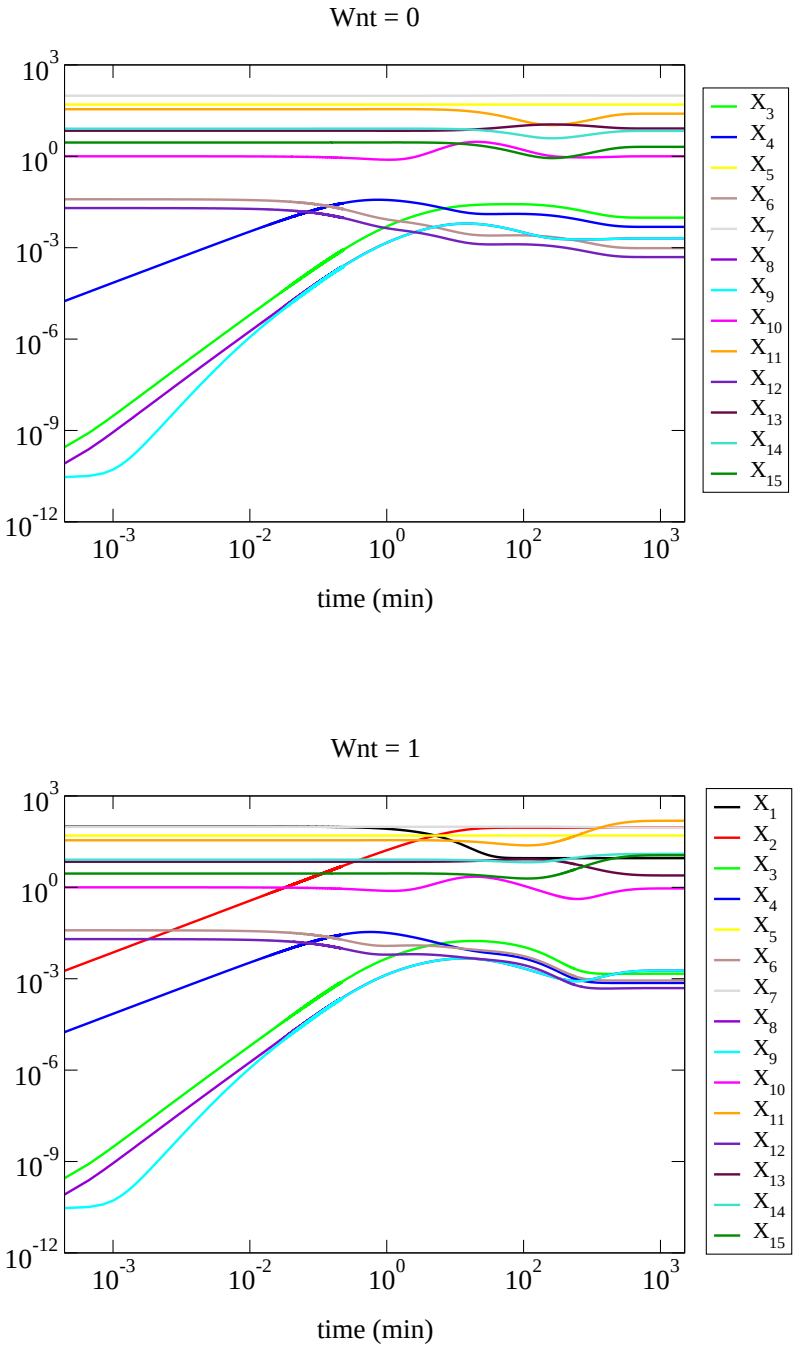

Figure 3.3: The temporal evolution of the 15 concentrations of the system's proteins and protein complexes. Top: the reference state; the concentrations of X_1 and X_2 are constant at their initial values 100 nM and 0, respectively. Bottom: the stimulated state.

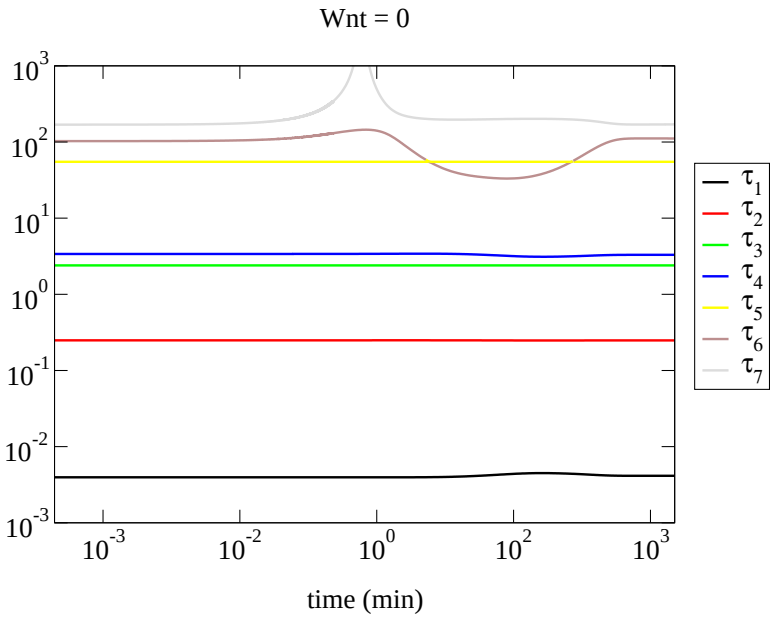

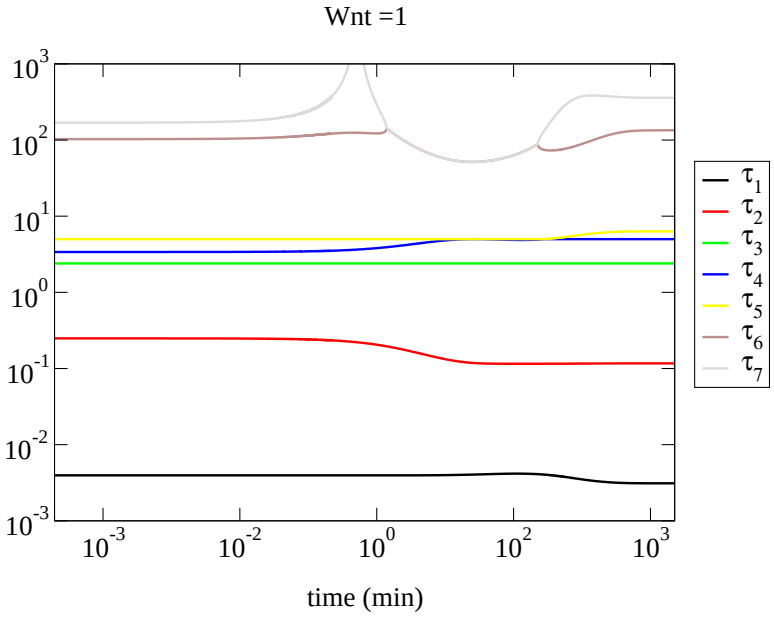

Figure 3.4: The temporal evolution of the 7 time scales of the system. Top: the reference state. Bottom: the stimulated state.

Chapter 4

CSP analysis on the *Wnt/β model*

The modified *Wnt* model, Table 3.4, will be analyzed with the *CSP* method in the *reference state* ($Wnt = 0$) and *stimulated state* ($Wnt = 1$). The *CSP* diagnostics will be discussed for both states. In the next sections (i) the 15 proteins (species) will be classified according to their relation to the fast dissipative time scales, (ii) the contribution of the 17 reactions (steps) in the model to the formation of the *SIM* will be investigated, (iii) the reactions contributing to the flow along the *SIM* will be identified and (iv) the reactions generating the fast time scales will be presented. The results in (i)-(iv) will be discussed separately and combined, in order to get a better insight for the dynamics of the model. The analysis will be restricted in the 7-dim. subspace of the state space, in which the solution of the modified *Wnt* model evolves. Inside this subspace, it will be shown that the number M of the fast processes that become exhausted changes with time.

4.1 The reference state

In this section, the case without Wnt stimulation ($Wnt = 0$) will be examined, so that the rates V_1, V_2 and V_3 are inactive and the X_1 and X_2 species do not participate see Tables 3.1 and 3.2.

Shown in Fig. (4.1) is the temporal evolution of the number M fast time scales of the modified *Wnt* model that are considered exhausted. The value of M was determined by requiring leading and second order accuracy in approximating the *SIM* and the slow model, according to the criteria discussed in Section 2.2. Let M_1 denote the number of the exhausted time scales determined by the criterion assuring leading order accuracy, Eq. (2.21), which requires the implementation of one $\mathbf{b}^r$-refinement and one $\mathbf{a}_r$-refinement. Let also M_2 denote the number of the exhausted time scales determined by the criterion assuring second order accuracy, Eq. (2.22), which requires the implementation of two $\mathbf{b}^r$-refinements and one $\mathbf{a}_r$-refinement. It is shown in Fig. (4.1) that M_1 and M_2 increase monotonically, from 1 to 4. The value of M cannot increase beyond that value since the three slower time scales remain close and no gap is developing among them. It is further demonstrated that M_1 increases sooner than M_2. This feature is reasonable, since higher order accuracy requires the solution to travel a longer distance along the *SIM*, so that the fast amplitudes $\mathbf{f}^r$ can decay further [10, 17].

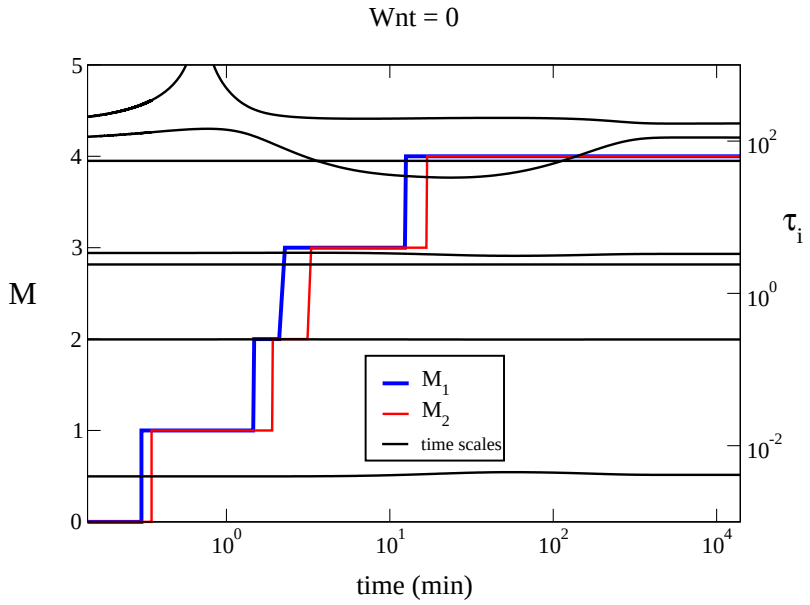

Figure 4.1: The evolution of the seven bounded time scales of the modified model in the reference state is displayed and it is shown that the number of fast time scales M increases with time; the time scales τ_i, $(i = 1, ..., 7)$ are denoted in black; M_1 (blue) denotes the number of the exhausted time scales when leading order accuracy is required; M_2 (red) denotes the number of the exhausted time scales when second order accuracy is required.

The species that associate with the exhausted fast time scales will be identified by the *CSP Pointer (PO)*, Eq.(2.26) and the reactions contributing to the formation of the M-dim. *SIM* will be identified by the *Participation Index (PI)*, Eq.(2.27). The reactions that drive the solution along the M-dim. *SIM* will be identified by the *Importance Index (II)*, Eq. (2.29) and the reactions that are responsible for the generation of the M exhausted fast time scales will be identified with the *Eigenvalue Participation Index (EPI)*, Eq.(2.33).

In the following, the dynamics of the modified *Wnt* model will be discussed at selected points in time. These points are located inside periods in which M stays constant. The dynamics that will be reported at these points are representative of the prevailing dynamics in these periods.

4.1.1 One exhausted mode

In the period $0.3 < t < 2.1$ *min*, $(M = 1)$, see Fig (4.1). The numerical results that will be reported in this section were computed at $t = 1.65$ min. These results did not changed significantly during the period in which $M = 1$, so that the conclusions that will be reached are valid throughout this period.

Table 4.1 shows that the pointed variable is the concentration of *(β-catenin*/APC*/Axin* /GSK3)* complex.

Table 4.2 shows that the reactions 9 and 10 are those that contribute the most to the generation of the $4 + M = 5$-dim. *SIM*; i.e., $V_9 - V_{10} \approx 0$. Given that the *PO* identifies the concentration

Table 4.1: Proteins and protein complexes indicated by *CSP Pointer* (PO), in the case where $M = 1$; bold indicates the species pointed the most.

M	Proteins and protein complexes	CSP Pointer
1	(**β-catenin*/APC*/Axin*/GSK3)**	**0.81**
	(β-catenin/APC*/Axin*/GSK3)	0.18

of *(β-catenin*/APC*/Axin*/GSK3)* (X_9) and the *PI* identifies reactions 9 and 10, it follows that this exhausted CSP mode relates to the *Quasi Steady State* of the pointed variable, since according to Table 3.4 $\dot{X}_9 = V_9 - V_{10}$.

Table 4.2: Proteins and protein complexes indicated by *CSP Pointer* are shown in column 3 (most pointed marked bold); reactions exhibiting *Participation Indices* greater than 5% are listed in column 4 (those providing PI's greater than 15% are marked by bold); reactions with + sign equilibrate with those with the - sign.

M	Amplitude of exhausted modes	Proteins and protein complexes	Reactions
1	f^1	(**β-catenin*/APC*/Axin*/GSK3)**,	**9**(0.5), **-10**(-0.5)
		(β-catenin/APC*/Axin*/GSK3)	

Table 4.3 lists the significant contributors for the generation of λ_1; i.e., those that exhibit the largest EPIs. It is shown that the contribution to the largest eigenvalue λ_1 is 81% of reaction 10 and 18% by reaction 9. Both of these reactions have to do with the concentration of *(β-catenin*/APC*/Axin*/GSK3)*. This suggests that the speed by which the fastest mode becomes exhausted, ($f^1 \approx 0$) has to do mainly with the dissociation of the phosphorylated *β-catenin* (V_{10}) and lesser by the degradation of the phosphorylated *β-catenin* (V_9) .

Table 4.3: Proteins and protein complexes indicated by *CSP Pointer* are shown in column 3 (most pointed marked bold); reactions exhibiting *Eigenvalue participation index (EPI)* greater than 5% are listed in column 4 (those providing EPI's greater than 15% are marked by bold)

M	Fast eigenvalues	Proteins and protein complexes	Reactions
1	λ_1	(**β-catenin*/APC*/Axin*/GSK3)**,	**-9**(-0.18), **-10**(-0.81)
		(β-catenin/APC*/Axin*/GSK3)	

The reactions that contribute to the slow evolution of the system on the 5-dim. *SIM* are depicted in column 2 of Table 4.4. These are reactions that exhibit the largest *II*s. The rate of change of these 8 proteins and protein complexes along the *SIM* are determined by the reaction rates indicated in column 3. The reactions that provide the most significant contribution are 4, 6, 9,

Table 4.4: Reactions providing non-negligible contribution to selected components of $\mathbf{g}_{slow}$, identified by the *Importance index (II)* Eq.(2.29). Only reactions exhibiting IIs greater than 1% are shown. Those providing IIs greater than 15% are indicated by bold. Reactions with the +(-) sign tend to increase (decrease) the concentration of the related protein or protein and protein complexes.

Proteins and protein complexes	Reactions	Rate of change
(APC/Axin*/GSK3)*	**4**, -5, 9, -12	$\frac{d[(APC^*/Axin^*/GSK3)]}{dt} \approx f(+\mathbf{V_4}, -V_5, +V_9, -V_{12})$
(APC/Axin/GSK3)	-4, 5, **6f**, **-6b**	$\frac{d[(APC/Axin/GSK3)]}{dt} \approx f(-V_4, +V_5, +\mathbf{V_6})$
GSK3	**-6f**, **6b**	$\frac{d[GSK3]}{dt} \approx f(-\mathbf{V_6})$
(APC/Axin)	**-6f**, **6b**	$\frac{d[(APC/Axin)]}{dt} \approx f(-\mathbf{V_6})$
APC	-6f, **9**, **-12**, 6b	$\frac{d[APC]}{dt} \approx f(+\mathbf{V_9}, -\mathbf{V_{12}}, -V_6)$
(β-catenin/APC/Axin*/GSK3)*	**4**, -5	$\frac{d[(\beta\text{-}catenin/APC^*/Axin^*/GSK3)]}{dt} \approx f(+\mathbf{V_4}, -V_5)$
*β-catenin**	**9**, **-11**	$\frac{d[\beta\text{-}catenin^*]}{dt} \approx f(+\mathbf{V_9}, -\mathbf{V_{11}})$
β-catenin	**-9**, **12**	$\frac{d[\beta\text{-}catenin]}{dt} \approx f(-\mathbf{V_9}, +\mathbf{V_{12}})$

11 and 12. These reactions have to do with (i) phosphorylation of *Axin* and *APC* (4), (ii) binding of *GSK3* to the *(APC/Axin)* complex and dissociation of *GSK3* from the destruction complex (6), (iii) phosphorylation of *β-catenin* (9), (iv) degradation of phosphorylated *β-catenin* (11) and (v) synthesis of *β-catenin* (12).

4.1.2 Two exhausted modes

At time $2.2 < t < 3.8\ min$, $(M = 2)$, see Fig (4.1). The numerical results that will be reported in this section were computed at $t = 3.35\ min$. The results at $t = 3.35\ min$ are valid thoughtout the period in which $M = 2$.

Table 4.5 shows that the two pointed variables are the concentration of *(β-catenin*/APC*/Axin* /GSK3)* and the concentration of *(APC/Axin)*.

Table 4.5: Proteins and protein complexes indicated by *CSP Pointer (PO)*, in the case where $M = 2$; bold indicates the species pointed the most

M	Proteins and protein complexes	CSP Pointer
1	**(β-catenin*/APC*/Axin*/GSK3)**	**0.82**
	(β-catenin/APC/Axin*/GSK3)*	0.18
2	**(APC/Axin)**	**0.73**
	(APC/Axin/GSK3)	0.25

Table 4.6 shows that the reactions that contribute the most to the generation of the $4 + M$ = 6-dim. *SIM* are: (i) reactions 9 and 10 for the first exhausted mode and (ii) reactions $6f$ and $6b$ for the second exhausted mode . Given that the *PO* identifies the concentration of *(β-catenin*/APC*/Axin*/GSK3)* (X_9) and the *PI* identifies reactions 9 and 10, it follows that the first *CSP* exhausted mode relates to the *Quasi Steady State* of the pointed variable, since according to Table 3.4 $\dot{X}_9 = V_9 - V_{10}$. The *PO* identifies the concentration of *(APC/Axin)* and the *PI* identifies reactions $6f$ and $6b$, it follows that the V_{6f} and V_{6b} equilibrate so that we can assume that the *PEA* is valid for the reaction 6, $V_{6f} - V_{6b} \approx 0$.

Table 4.6: Proteins and protein complexes indicated by *CSP Pointer* are shown in column 3 (most pointed marked bold); reactions exhibiting *Participation Indices* greater than 5% are listed in column 4 (those providing PI's greater than 15% are marked by bold); reactions with + sign equilibrate with those with the - sign.

M	Amplitude of exhausted modes	Proteins and protein complexes	Reactions
1	f^1	(**β-catenin*/APC*/Axin*/GSK3**), (β-catenin/APC*/Axin*/GSK3)	**9**(0.5), **-10**(-0.5)
2	f^2	**(APC/Axin)**, (APC*/Axin*/GSK3)	**-6f**(-0.48), **6b**(0.46)

Table 4.7 lists the significant contributors for the generation of λ_1 and λ_2. It is shown that the contribution to the largest eigenvalue λ_1 is 82% by reaction 10 and 18% by reaction 9. Both of these reactions have to do with the concentration of *(β-catenin*/APC*/Axin*/GSK3)*. This suggests that the speed by which the fastest mode becomes exhausted, ($f^1 \approx 0$) has to do mainly with the dissociation of the phosphorylated *β-catenin* (V_{10}) and lesser by the degradation of the phosphorylated *β-catenin* (V_9) . The contribution to λ_2 is 73% of reaction $6f$ and 23% by reaction $6b$. The forward reaction ($6f$) has to do with the synthesis of *(APC/Axin/GSK3)* from *GSK3* and *(APC/Axin)* and the backward reaction ($6b$) has to do with the degradation of *(APC/Axin/GSK3)*. So the speed by which the second fast mode becomes exhausted ($f^2 \approx 0$) has to do mainly with the speed that *(APC/Axin)* produced and lesser by the speed it is consumed.

The reactions that contribute to the slow evolution of the system on the 6-dimensional *SIM* are depicted in column 2 of Table 4.8. These are reactions that exhibit the largest *II*s. The rate of change of these 7 protein and protein complexes along the *SIM* are determined by the reactions indicated in column 3. The reactions that provide significant contribution to the slow components are 4, 5, 9, 11 and 12 that have to do with (i) phosphorylation of *Axin* and *APC* (4), (ii) dephosphorylation of *Axin* and *APC* (5), (iii) phosphorylation of *β-catenin* (9), (iv) degradation of phosphorylated *β-catenin* (11) and (v) synthesis of *β-catenin* (12). We observe that given the rising equilibria of $6f$ and $6b$ namely the equilibria between the binding and the dissociation of *GSK3* to and from the *(APC/Axin)* complex reaction 5 arises to define the slow evolution on the *SIM*.

Table 4.7: Proteins and protein complexes indicated by *CSP Pointer* are shown in column 3 (most pointed marked bold); reactions exhibiting *Eigenvalue participation index (EPI)* greater than 5% are listed in column 4 (those providing EPI's greater than 15% are marked by bold)

M	Fast eigenvalues	Proteins and protein complexes	Reactions
1	λ_1	(**β-catenin*/APC*/Axin*/GSK3)**, (β-catenin/APC*/Axin*/GSK3)	**-9**(-0.18), **-10**(-0.82)
2	λ_2	**(APC/Axin)**, (APC*/Axin*/GSK3)	**-6f**(-0.73), **+6b**(0.23)

Table 4.8: Reactions providing non-negligible contribution to selected components of $\mathbf{g}_{slow}$, identified by the *Importance index (II)* Eq.(2.29). Only reactions exhibiting IIs greater than 1% are shown. Those providing IIs greater than 15% are indicated by bold. Reactions with the +(-) sign tend to increase (decrease) the concentration of the related protein or protein and protein complexes.

Proteins and protein complexes	Reactions	Rate of change
(APC/Axin*/GSK3)*	**4**, **-5**, 9	$\frac{d[(APC^*/Axin^*/GSK3)]}{dt} \approx f(\mathbf{V_4}, -\mathbf{V_5}, +V_9)$
(APC/Axin/GSK3)	**-4**, **5**, -15	$\frac{d[(APC/Axin/GSK3)]}{dt} \approx f(-\mathbf{V_4}, +\mathbf{V_5}, -V_{15})$
GSK3	**-4**, **5**, -14, 15	$\frac{d[GSK3]}{dt} \approx f(-\mathbf{V_4}, +\mathbf{V_5}, -V_{14}, +V_{15})$
APC	-4, **9**, **-12**	$\frac{d[APC]}{dt} \approx f(-V_4, +\mathbf{V_9}, -\mathbf{V_{12}})$
(β-catenin/APC/Axin*/GSK3)*	**4**, **-5**, -9, 12	$\frac{d[(\beta\text{-}catenin/APC^*/Axin^*/GSK3)]}{dt} \approx f(+\mathbf{V_4}, -\mathbf{V_5}, -V_9, +V_{12})$
*β-catenin**	**9**, **-11**	$\frac{d[\beta\text{-}catenin^*]}{dt} \approx f(+\mathbf{V_9}, -\mathbf{V_{11}})$
β-catenin	**-9**, **12**	$\frac{d[\beta\text{-}catenin]}{dt} \approx f(-\mathbf{V_9}, +\mathbf{V_{12}})$

4.1.3 Three exhausted modes

At time $4 < t < 27\ min$, $(M = 3)$, see Fig (4.1). The numerical results that will be reported in this section were computed at $t = 21.24\ min$. The results at $t = 21.24\ min$ are valid thoughtout the period in which $M = 3$.

Table 4.9 shows that the three pointed variables are the concentrations of *(β-catenin*/APC* /Axin*/GSK3)*, *(APC/Axin)* and *β-catenin**.

Table 4.10 shows that the reactions that contribute the most to the generation of the $4+M = 6$-dim. *SIM* are: (i) reactions 9 and 10 for the first exhausted mode, (ii) reactions $6f$ and $6b$ for the second exhausted mode and (iii) 4, 5, 10 and 11 for the third exhausted mode. Given that the *PO* identifies the concentration of *(β-catenin*/APC*/Axin*/GSK3)* (X_9) and the *PI* identifies reactions 9 and 10, it follows that the first *CSP* mode relates to the *Quasi Steady State* of the pointed variable, since according to Table 3.4 $\dot{X}_9 = V_9 - V_{10}$. The *PO* identifies the concentration of *(APC/Axin)* (X_6) and the *PI* identifies reactions $6f$ and $6b$, it follows that the V_{6f} and V_{6b} equilibrate so that we can assume that the *PEA* is valid for the reaction 6, $V_{6f} - V_{6b} \approx 0$. The *PO*

Table 4.9: Proteins and protein complexes indicated by *CSP Pointer (PO)*, in the case where M=3; bold indicates the species pointed the most

M	Proteins and protein complexes	CSP Pointer
1	(**β-catenin*/APC*/Axin*/GSK3)**	**0.86**
	(β-catenin/APC*/Axin*/GSK3)	0.14
2	**(APC/Axin)**	**0.74**
	(APC/Axin/GSK3)	0.25
3	**β-catenin***	**1.00**

identifies the concentration of *β-catenin** (X_{10}) and the *PI* indicates that there is an equilibria between reactions V_{10} and V_{11} and V_4 and V_5 so that $-V_4 + V_5 + V_{10} - V_{11} \approx 0$.

Table 4.10: Proteins and protein complexes indicated by *CSP Pointer* are shown in column 3 (most pointed marked bold); reactions exhibiting *Participation Indices* greater than 5% are listed in column 4 (those providing PI's greater than 15% are marked by bold); reactions with + sign equilibrate with those with the - sign.

M	Amplitude of exhausted modes	Proteins and protein complexes	Reactions
1	f^1	(**β-catenin*/APC*/Axin*/GSK3)**, (β-catenin/APC*/Axin*/GSK3)	**9**(0.5), **-10**(0.5)
2	f^2	**(APC/Axin)**, (APC*/Axin*/GSK3)	**-6f**(-0.46), **6b**(0.46)
3	f^3	**β-catenin***	-4(-0.13), 5(0.14), **10**(0.34), **-11**(-0.35)

Table 4.11 lists the significant contributors for the generation of λ_1, λ_2 and λ_3. It is shown that the contribution to the first two eigenvalues are the same reactions as in the case for the two exhausted modes, Section 4.1.2. The contribution to λ_3 is by reaction 11. The reaction has to do with the degradation of *β-catenin** by the destruction complex and the proteasome respectively. This suggests that the speed by which the third fast mode becomes exhausted ($f^3 \approx 0$) has to do with the speed by *β-catenin** is degraded.

The reactions that contribute to the slow evolution of the system on the 7-dim. *SIM* are depicted in column 2 of Table 4.12. These are reactions that exhibit the largest *II*s. The rate of change of these 6 proteins and protein complexes along the *SIM* are determined by the reactions indicated in column 3. The reactions that provide significant contribution to the slow components are 4, 5, 9 and 12 that have to do with (i) phosphorylation of *Axin* and *APC*, (ii) dephosphorylation of

Table 4.11: Proteins and protein complexes indicated by *CSP Pointer* are shown in column 3 (most pointed marked bold); reactions exhibiting *Eigenvalue participation index (EPI)* greater than 5% are listed in column 4 (those providing EPI's greater than 15% are marked by bold)

M	Fast eigenvalues	Proteins and protein complexes	Reactions
1	λ_1	(**β-catenin*/APC*/Axin*/GSK3)**, (β-catenin/APC*/Axin*/GSK3)	**-9**(-0.14), **-10**(-0.86)
2	λ_2	**(APC/Axin)**, (APC*/Axin*/GSK3)	**-6f**(-0.74), **+6b**(0.23)
3	λ_3	**β-catenin***	**-11**(-1.0)

Table 4.12: Reactions providing non-negligible contribution to selected components of $\mathbf{g}_{slow}$, identified by the *Importance index (II)* Eq.(2.29). Only reactions exhibiting IIs greater than 1% are shown. Those providing IIs greater than 15% are indicated by bold. Reactions with the +(-) sign tend to increase (decrease) the concentration of the related protein or protein and protein complexes.

Proteins and protein complexes	Reactions	Rate of change
(APC/Axin*/GSK3)*	**4**, **-5**, 9, -12	$\frac{d[(APC^*/Axin^*/GSK3)]}{dt} \approx f(+\mathbf{V_4}, -\mathbf{V_5}, +V_9, -V_{12})$
(APC/Axin/GSK3)	**-4**, **5**, 14, -15	$\frac{d[(APC/Axin/GSK3)]}{dt} \approx f(-\mathbf{V_4}, +\mathbf{V_5}, +V_{14}, -V_{15})$
GSK3	**-4**, **5**, -14, 15	$\frac{d[GSK3]}{dt} \approx f(-\mathbf{V_4}, +\mathbf{V_5}, -V_{14}, +V_{15})$
APC	**9**, **-12**	$\frac{d[APC]}{dt} \approx f(+\mathbf{V_9}, -\mathbf{V_{12}})$
(β-catenin/APC/Axin*/GSK3)*	**4**, **-5**, -9, 12	$\frac{d[(\beta\text{-}catenin/APC^*/Axin^*/GSK3)]}{dt} \approx f(+\mathbf{V_4}, -\mathbf{V_5}, -V_9, +V_{12})$
β-catenin	**-9**, **12**	$\frac{d[\beta\text{-}catenin]}{dt} \approx f(-\mathbf{V_9}, +\mathbf{V_{12}})$

Axin and *APC*, (iii) phosphorylation of *β-catenin* and (iv) synthesis of *β-catenin*. Given the rising equilibria of reactions 10 and 11 namely dissociation of phosphorylated *β-catenin* and degradation of phosphorylated *β-catenin* reaction 11 has negligible role in the slow evolution along the *SIM*.

4.1.4 Four exhausted modes

At time $28 < t < 5000$ *min*, ($M = 4$), see Fig (4.1). The numerical results that will be reported in this section were computed at $t = 2600$ *min*. The results at $t = 2600$ *min* are valid thoughtout the period in which $M = 3$.

Table 4.13 shows that the four pointed variables are the concentrations of *(β-catenin*/APC* /Axin*/GSK3)*, *(APC/Axin)*, *β-catenin** and *(APC/Axin/GSK3)*.

Table 4.14 shows that the reactions that contribute the most to the generation of the $4+M = 8$-dim. *SIM* are (i) reactions 9 and 10 for the first exhausted mode, (ii) reactions $6f$ and $6b$ for the second exhausted mode, (iii) reactions 10 and 11 for the third exhausted mode and (iv) reactions 4, 5, $6f$ and $6b$ for the fourth exhausted mode. Given the first two exhausted modes the results are

Table 4.13: Proteins and protein complexes indicated by *CSP Pointer (PO)*; bold indicates the species pointed the most

M	Proteins and protein complexes	CSP Pointer
1	(**β-catenin*/APC*/Axin*/GSK3)**	**0.85**
	(β-catenin/APC*/Axin*/GSK3)	0.15
2	**(APC/Axin)**	**0.74**
	(APC/Axin/GSK3)	0.25
3	**β-catenin***	**1.00**
4	**(APC/Axin/GSK3)**	**0.52**
	(APC*/Axin*/GSK3)	0.29
	(APC/Axin)	0.15

the same as in Section 4.1.4, for the third exhausted mode *PO* identifies the concentration of *β-catenin** (X_{10}) and the *PI* identifies reactions 10 and 11, it follows that the third *CSP* mode relates to the *Quasi Steady State* of the pointed variable, since according to Table 3.4 $\dot{X}_{10} = V_{10} - V_{11}$. For the fourth exhausted mode the *PO* identifies *(APC/Axin/GSK3)* (X_4) and the *PI* produces the equilibration $V_4 \approx V_5$, given the equilibration $V_{6f} \approx V_{6b}$ and that $V_3 = 0$ we can assume that *(APC/Axin/GSK3)* is amenable to *QSSA*, since according to Table 3.4 $\dot{X}_4 = -V_3 - V_4 + V_5 + V_6$

Table 4.14: Proteins and protein complexes indicated by *CSP Pointer* are shown in column 3 (most pointed marked bold); reactions exhibiting *Participation Indices* greater than 5% are listed in column 4 (those providing PI's greater than 15% are marked by bold); reactions with + sign equilibrate with those with the - sign.

M	Amplitude of exhausted modes	Proteins and protein complexes	Reactions
1	f^1	(**β-catenin*/APC*/Axin*/GSK3)**, (β-catenin/APC*/Axin*/GSK3)	**9**(0.5), **-10**(-0.5)
2	f^2	**(APC/Axin)**, (APC*/Axin*/GSK3)	**-6f**(-0.49), **6b**(0.49)
3	f^3	**β-catenin***	**10**(0.5), **-11**(-0.48)
4	f^4	**(APC/Axin/GSK3)**, (APC*/Axin*/GSK3), (APC/Axin)	-4(-0.11), 5(0.11), **-6f**(0.38), **6b**(-0.38)

Table 4.15 lists the significant contributors for the generation of λ_1, λ_2, λ_3 and λ_4. It is shown that the contribution to the first three eigenvalues are the same reactions as in the case for the three exhausted modes, Section 4.1.3. The contribution to λ_4 is 48% by reaction 4, 21% by reaction 5 and 10% by reactions $6f$ and $6b$. Reaction 4 has to do with the phosphorylation of *(APC/Axin/GSK3)*, reaction 5 has to do with the dephosphorylation of *(APC*/Axin*/GSK3)*. Reactions $6f$ and $6b$ have to do with the synthesis of *(APC/Axin/GSK3)* from (*GSK3* and *(APC/Axin)*) and degradation of *(APC/Axin/GSK3)* respectively.

Table 4.15: Proteins and protein complexes indicated by *CSP Pointer* are shown in column 3 (largest pointed marked bold); reactions exhibiting *Eigenvalue participation index (EPI)* greater than 5% are listed in column 4 (those providing EPI's greater than 15% are marked by bold)

M	Fast eigenvalues	Proteins and protein complexes	Reactions
1	λ_1	(**β-catenin*/APC*/Axin*/GSK3)**, (β-catenin/APC*/Axin*/GSK3)	**-9**(-0.15), **-10**(-0.85)
2	λ_2	**(APC/Axin)**, (APC*/Axin*/GSK3)	**-6f**(-0.73), **+6b**(0.23)
3	λ_3	**β-catenin***	**-11**(-1.0)
4	λ_4	**(APC/Axin/GSK3)**, (APC*/Axin*/GSK3), (APC/Axin)	**-4**(-0.48), **-5**(-0.21), -6f(-0.11), -6b(-10)

The reactions that contribute to the slow evolution of the system on the 8-dim. *SIM* are depicted in column 2 of Table 4.16. These are reactions that exhibit the largest IIs. The rate of change of these 7 proteins and protein complexes along the *SIM* are determined by the reactions indicated in column 3. The reactions that provide significant contribution to the slow components are 9, 12, 14 and 15 that have to do with (i) phosphorylation of β-*catenin*, (ii) synthesis of β-*catenin*, (iii) synthesis of *Axin* and (iv) degradation of *Axin* respectively. Given the rising equilibria of reactions 4 and 5 namely phosphorylation of *Axin* and *APC*, dephosphorylation of *Axin* and *APC* reactions 14 and 15 arise to provide significant role in the slow evolution along the *SIM*.

Table 4.16: Reactions providing non-negligible contribution to selected components of $\mathbf{g}_{slow}$, identified by the *Importance index (II)* Eq.(2.29). Only reactions exhibiting IIs greater than 1% are shown. Those providing IIs greater than 15% are indicated by bold. Reactions with the +(-) sign tend to increase (decrease) the concentration of the related protein or protein and protein complexes.

Proteins and protein complexes	Reactions	Rate of change
(APC/Axin*/GSK3)*	**9**, **-12**, **14**, **-15**	$\frac{d[(APC^*/Axin^*/GSK3)]}{dt} \approx f(+\mathbf{V_9}, -\mathbf{V_{12}}, +\mathbf{V_{14}}, -\mathbf{V_{15}})$
GSK3	**9**, **-12**, **-14**, **15**	$\frac{d[GSK3]}{dt} \approx f(+\mathbf{V_9}, -\mathbf{V_{12}}, -\mathbf{V_{14}}, +\mathbf{V_{15}})$
APC	**9**, **-12**	$\frac{d[APC]}{dt} \approx f(+\mathbf{V_9}, -\mathbf{V_{12}})$
(β-catenin/APC/Axin*/GSK3)*	**-9**, **12**, +14, -15	$\frac{d[(\beta\text{-}catenin/APC^*/Axin^*/GSK3)]}{dt} \approx f(-\mathbf{V_9}, +\mathbf{V_{12}}, +V_{14}, -V_{15})$
β-catenin	**-9**, **12**	$\frac{d[\beta\text{-}catenin]}{dt} \approx f(-\mathbf{V_9}, +\mathbf{V_{12}})$

4.2 The stimulated state

Here, the case with Wnt stimulation ($Wnt = 1$) will be examined, so in contrast with the reference state the rates V_1, V_2 and V_3 are active and the X_1 and X_2 species participate.

Shown in Fig. (4.2) is the temporal evolution of the number M fast time scales of the modified *Wnt* model that are considered exhausted. The value of M was determined by requiring leading and second order accuracy in approximating the *SIM* and the slow model, according to the criteria discussed in Section 2.2. M_1 denotes the number of the exhausted time scales determined by the criterion assuring leading order accuracy, Eq. (2.21), which requires the implementation of one $\mathbf{b}^r$-refinement and one $\mathbf{a}_r$-refinement. M_2 denote the number of the exhausted time scales determined by the criterion assuring second order accuracy, Eq. (2.22), which requires the implementation of two $\mathbf{b}^r$-refinements and one $\mathbf{a}_r$-refinement. It is shown in Fig. (4.2) that M_1 and M_2 increase monotonically, as in the reference state shown in Fig. (4.1), now from 1 to 5. The value of M cannot increase beyond that value since no gap develops between that two slowest time scales. It is also demonstrated that M_1 increases sooner than M_2. This feature was explained in the reference state, Section 4.1.

The results from the *CSP* diagnostics will be presented in the same way as in the reference state. The species that associate with the exhausted fast time scales will be identified by the *CSP Pointer (PO)*, Eq.(2.26) and the reactions contributing to the formation of the M-dim. *SIM* will be identified by the *Participation Index (PI)*, Eq.(2.27). The reactions that drive the solution along the M-dim. *SIM* will be identified by the *Importance Index (II)*, Eq. (2.29) and the reactions that are responsible for the generation of the M exhausted fast time scales will be identified with the *Eigenvalue Participation Index (EPI)*, Eq.(2.33).

In the following, the dynamics of the modified *Wnt* model will be discussed at selected points in time as in the reference state, Section 4.1.

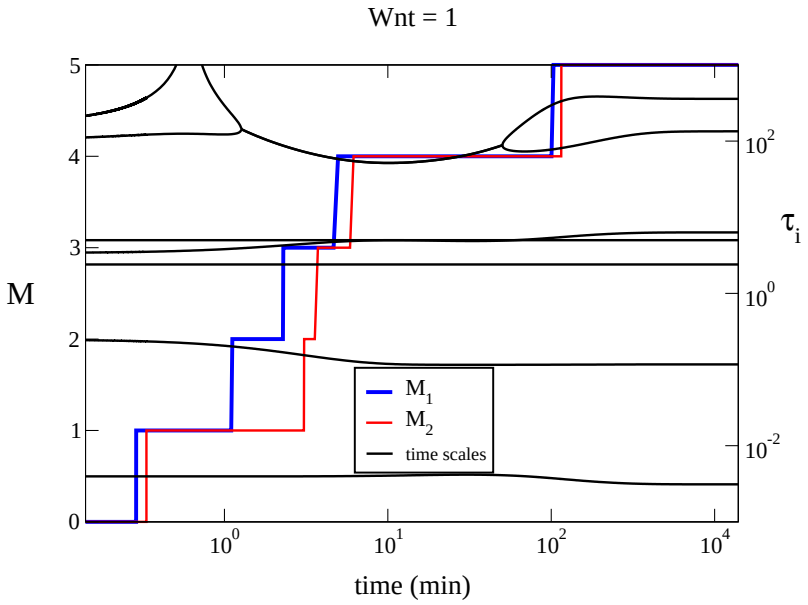

Figure 4.2: The evolution of the seven bounded time scales of the modified model in the stimulated state is displayed and it is shown that the number of fast time scales M increases with time; the time scales τ_i, $(i = 1, ..., 7)$ are denoted in black; M_1 (blue) denotes the number of the exhausted time scales when leading order accuracy is required; M_2 (red) denotes the number of the exhausted time scales when second order accuracy is required.

4.2.1 One exhausted mode

At time $0.2 < t < 3.7$ *min*, $(M = 1)$, see Fig (4.2). The numerical results that will be reported in this section were computed at $t = 3.35$ *min*. The results at $t = 3.35$ *min* are valid throughout the period in which $M = 1$.

Table 4.17 shows that the pointed variable is the concentration of *(β-catenin*/APC*/Axin* /GSK3)*.

Table 4.17: Proteins and protein complexes indicated by *CSP Pointer* in the stimulated state; bold indicates the species pointed the most

M	Proteins and protein complexes	CSP Pointer
1	**(β-catenin*/APC*/Axin*/GSK3)**	**0.81**
	(β-catenin/APC*/Axin*/GSK3)	0.18

Table 4.18 shows that the reactions 9 and 10 are those that contribute the most to the generation of the $4 + M = 5$-dim. *SIM*; i.e., $V_9 - V_{10} \approx 0$. Given that the *PO* identifies the concentration

of *(β-catenin*/APC*/Axin*/GSK3)* (X_9) and the *PI* identifies reactions 9 and 10, it follows that this exhausted CSP mode relates to the *Quasi Steady State* of the pointed variable, since according to Table 3.4 $\dot{X}_9 = V_9 - V_{10}$.

Table 4.18: Proteins and protein complexes indicated by *CSP Pointer* are shown in column 3 (most pointed marked bold); reactions exhibiting *Participation Indices* greater than 5% are listed in column 4 (those providing PI's greater than 15% are marked by bold); reactions with + sign equilibrate with those with the - sign.

M	Amplitude of exhausted modes	Proteins and protein complexes	Reactions
1	f^1	(**β-catenin*/APC*/Axin*/GSK3**), (β-catenin/APC*/Axin*/GSK3)	**9**(0.5), **-10**(-0.5)

Table 4.19 lists the significant contributors for the generation of λ_1; i.e., those that exhibit the largest EPIs. It is shown that the contribution to the largest eigenvalue λ_1 is 81% of reaction 10 and 18% by reaction 9. Both of these reactions have to do with the concentration of *(β-catenin*/APC*/Axin*/GSK3)*. This suggests that the speed by which the fastest mode becomes exhausted, ($f^1 \approx 0$) has to do mainly with the dissociation of the phosphorylated *β-catenin* (V_{10}) and lesser by the degradation of the phosphorylated *β-catenin* (V_9) .

Table 4.19: Proteins and protein complexes indicated by *CSP Pointer* are shown in column 3 (most pointed marked bold); reactions exhibiting *Eigenvalue participation index (EPI)* greater than 5% are listed in column 4 (those providing EPI's greater than 15% are marked by bold)

M	Fast eigenvalues	Proteins and protein complexes	Reactions
1	λ_1	(**β-catenin*/APC*/Axin*/GSK3**), (β-catenin/APC*/Axin*/GSK3)	**-9**(-0.18), **-10**(-0.81)

The reactions that contribute to the slow evolution of the system on the 5-dim. *SIM* are depicted in column 2 of Table 4.20. These are reactions that exhibit the largest *II*s. The rate of change of these 10 proteins and protein complexes along the *SIM* are determined by the reaction rates indicated in column 3. The reactions that provide the most significant contribution are 1, 3, 4, 5, 6, 9, 11 and 12. These reactions have to do with (i) the activation of *Dsh* by the *Wnt* signal (reaction 1), (ii) the dissociation of *GSK3* from the destruction complex (reaction 3), (iii) phosphorylation of *Axin* and *APC*(reaction 4), (iv) dephosphorylation of *Axin* and *APC* (reaction 5), (v) binding of *GSK3* to the *(APC/Axin)* complex and dissociation of *GSK3* from the destruction complex (reaction 6), (vi) phosphorylation of *β-catenin* (reaction 9), (vii) degradation of phosphorylated *β-catenin* (reaction 11) and (viii) synthesis of *β-catenin* (reaction 12).

Table 4.20: Reactions providing non-negligible contribution to selected components of $\mathbf{g}_{slow}$, identified by the *Importance index (II)* Eq.(2.29). Only reactions exhibiting IIs greater than 1% are shown. Those providing IIs greater than 15% are indicated by bold. Reactions with the +(-) sign tend to increase (decrease) the concentration of the related protein or protein and protein complexes.

Proteins and protein complexes	Reactions	Rate of change
Dsh_i	**-1**, 2	$\frac{d[Dsh_i]}{dt} \approx f(-\mathbf{V_1}, +V_2)$
Dsh_a	**1**, -2	$\frac{d[Dsh_a]}{dt} \approx f(+\mathbf{V_1}, -V_2)$
(APC/Axin*/GSK3)*	**4**, **-5**, 9	$\frac{d[(APC^*/Axin^*/GSK3)]}{dt} \approx f(+\mathbf{V_4}, -\mathbf{V_5}, +V_9)$
(APC/Axin/GSK3)	**-3**, -4, **6f**, **-6b**	$\frac{d[(APC/Axin/GSK3)]}{dt} \approx f(-\mathbf{V_3}, -V_4, +\mathbf{V_6})$
GSK3	**3**, **-6f**, **6b**	$\frac{d[GSK3]}{dt} \approx f(+V_3, -\mathbf{V_6})$
(APC/Axin)	**3**, **-6f**, **6b**	$\frac{d[(APC/Axin)]}{dt} \approx f(+\mathbf{V_3}, -\mathbf{V_6})$
APC	3, **-6f**, **9**, **-12**, 6b	$\frac{d[APC]}{dt} \approx f(+V_3, -\mathbf{V_6}, +\mathbf{V_9}, -\mathbf{V_{12}})$
(β-catenin/APC/Axin*/GSK3)*	**4**, **-5** -9, 12	$\frac{d[(\beta\text{-catenin}/APC^*/Axin^*/GSK3)]}{dt} \approx f(+\mathbf{V_4}, -\mathbf{V_5}, -V_9, +V_{12})$
*β-catenin**	**9**, **-11**	$\frac{d[\beta\text{-catenin}^*]}{dt} \approx f(+\mathbf{V_9}, -\mathbf{V_{11}})$
β-catenin	**-9**, **12**	$\frac{d[\beta\text{-catenin}]}{dt} \approx f(-\mathbf{V_9}, +\mathbf{V_{12}})$

4.2.2 Two exhausted modes

At time $t = 3.7 < t < 4.5\ min$, $(M = 2)$, see Fig (4.2). The numerical results that will be reported in this section were computed at $t = 4.22\ min$. The results at $t = 4.22\ min$ are valid throughout the period in which $M = 2$.

Table 4.21 shows that the pointed variables are the concentration of *(β-catenin*/APC*/Axin* /GSK3)* and *(APC/Axin/GSK3)*.

Table 4.21: Proteins and protein complexes indicated by *CSP Pointer* in the stimulated state; bold indicates the species pointed with the larger contribution

M	Proteins and protein complexes	CSP Pointer contribution
1	**(β-catenin*/APC*/Axin*/GSK3)**	**0.81**
	(β-catenin/APC*/Axin*/GSK3)	0.18
2	**(APC/Axin/GSK3)**	**0.55**
	(APC/Axin)	0.44

Table 4.22 shows that the reactions that contribute the most to the generation of the $4 + M =$ 6-dim. *SIM* are: (i) reactions 9 and 10 for the first exhausted mode and (ii) reactions 3, $6f$

and $6b$ for the second exhausted mode . Given that the *PO* identifies the concentration of *(β-catenin*/APC*/Axin*/GSK3)* (X_9) and the *PI* identifies reactions 9 and 10, it follows that the first *CSP* mode relates to the *Quasi Steady State* of the pointed variable, since according to Table 3.4 $\dot{X}_9 = V_9 - V_{10}$. The *PO* identifies the concentration of *(APC/Axin/GSK3)* and the *PI* identifies reactions 3, $6f$ and $6b$, it follows that the V_3, V_{6f} and V_{6b} equilibrate.

Table 4.22: Proteins and protein complexes indicated by *CSP Pointer* are shown in column 3 (largest pointed marked bold); reactions exhibiting *Participation Indices* greater than 5% are listed in column 4 (those providing PI's greater than 15% are marked by bold); reactions with + sign equilibrate with those with the - sign.

M	Amplitude of exhausted modes	Proteins and protein complexes	Reactions
1	f^1	(**β-catenin*/APC*/Axin*/GSK3)**, (β-catenin/APC*/Axin*/GSK3)	**9**(0.5), **-10**(-0.50)
2	f^2	**(APC/Axin/GSK3)**, (APC/Axin)	**-3**(-0.35), **6f**(0.47), -6b(-0.12)

Table 4.23 lists the significant contributors for the generation of λ_1 and λ_2. It is shown that the contribution to the largest eigenvalue λ_1 is 82% by reaction 10 and 18% by reaction 9. Both of these reactions have to do with the concentration of *(β-catenin*/APC*/Axin*/GSK3)*. This suggests that the speed by which the fastest mode becomes exhausted, ($f^1 \approx 0$) has to do mainly with the dissociation of the phosphorylated *β-catenin* (V_{10}) and lesser by the degradation of the phosphorylated *β-catenin* (V_9) . The contribution to λ_2 is 39% by reaction 3, 44% by reaction $6f$ and 13% by reaction $6b$. Reaction 3 has to do with the *Dsh*-mediated initiation of the release of *GSK3* from the destruction complex. The forward reaction ($6f$) has to do with the synthesis of *(APC/Axin/GSK3)* from *GSK3* and *(APC/Axin)* and the backward reaction ($6b$) has to do with the degradation of *(APC/Axin/GSK3)*. So the speed by which the second fast mode becomes exhausted ($f^2 \approx 0$) has to do mainly by the speed that *GSK3* and *(APC/Axin)* synthesize *(APC/Axin/GSK3)* lesser by the speed that *GSK3* is released from the destruction complex through *Dsh*-mediated initiation and in the smallest degree from the speed that *(APC/Axin/GSK3)* degrades and releases *GSK3*.

The reactions that contribute to the slow evolution of the system on the 6-dimensional *SIM* are depicted in column 2 of Table 4.24. These are reactions that exhibit the largest *II*s. The rate of change of these 9 protein and protein complexes along the *SIM* are determined by the reactions indicated in column 3. The reactions that provide significant contribution to the slow components are 1, 3, 4, $6f$, 9, 11 and 12 that have to do with the (i) activation of *Dsh* by the *Wnt* signal (reaction 1), (ii) dissociation of *GSK3* from the destruction complex (reaction 3), (iii) phosphorylation of *Axin* and *APC* (reaction 4), (iv) binding of *GSK3* to the *(APC/Axin)* complex (reaction $6f$), (v) phosphorylation of *β-catenin* (reaction 9), (vi) degradation of phosphorylated *β-catenin* (reaction 11) and (vi) synthesis of *β-catenin* (reaction 12).

Table 4.23: Proteins and protein complexes indicated by *CSP Pointer* are shown in column 3 (largest pointed marked bold); reactions exhibiting *Eigenvalue participation index (EPI)* greater than 5% are listed in column 4 (those providing EPI's greater than 15% are marked by bold)

M	Fast eigenvalues	Proteins and protein complexes	Reactions
1	λ_1	(**β-catenin*/APC*/Axin*/GSK3)**, (β-catenin/APC*/Axin*/GSK3)	**-9**(-0.18), **-10**(-0.82)
2	λ_2	**(APC/Axin/GSK3)**, (APC/Axin)	**-3**(-0.39), **-6f**(-0.44), **+6b**(0.13)

Table 4.24: Reactions providing non-negligible contribution to selected components of $\mathbf{g}_{slow}$, identified by the *Importance index (II)* Eq.(2.29). Only reactions exhibiting IIs greater than 1% are shown. Those providing IIs greater than 15% are indicated by bold. Reactions with the +(-) sign tend to increase (decrease) the concentration of the related protein or protein and protein complexes.

Proteins and protein complexes	Reactions	Rate of change
Dsh_i	**-1**, 2	$\frac{d[Dsh_i]}{dt} \approx f(-\mathbf{V_1}, +V_2)$
Dsh_a	**1**, -2	$\frac{d[Dsh_a]}{dt} \approx f(+\mathbf{V_1}, -V_2)$
(APC/Axin*/GSK3)*	**-3**, **4**, -5, **6f**, 9, 6b	$\frac{d[(APC^*/Axin^*/GSK3)]}{dt} \approx f(-\mathbf{V_3}, +\mathbf{V_4}, -V_5, +\mathbf{V_{6f}}, +V_9, +V_{6b})$
GSK3	**1**, -2, 3, **-4**, 5, **-6f**, **10**, 6b	$\frac{d[GSK3]}{dt} \approx f(+\mathbf{V_1}, -V_2, +V_3, -\mathbf{V_4}, +V_5, -\mathbf{V_{6f}}, +\mathbf{V_{10}}, +V_{6b})$
(APC/Axin)	**1**, -2, 3, **-4**, 5, **-6f**, -15, 6b	$\frac{d[(APC/Axin)]}{dt} \approx f(+\mathbf{V_1}, -V_2, +V_3, -\mathbf{V_4}, +V_5, -\mathbf{V_{6f}}, -V_{15}, +V_{6b})$
APC	**9**, **-12**, 15	$\frac{d[APC]}{dt} \approx f(+\mathbf{V_9}, -\mathbf{V_{12}}, +V_{15})$
(β-catenin/APC/Axin*/GSK3)*	**-3**, **4** -5, **6f**, 9, 6b	$\frac{d[(\beta\text{-}catenin/APC^*/Axin^*/GSK3)]}{dt} \approx f(-\mathbf{V_3}, +\mathbf{V_4}, -V_5, +\mathbf{V_{6f}}, +V_9, +V_{6b})$
*β-catenin**	**9**, **-11**	$\frac{d[\beta\text{-}catenin^*]}{dt} \approx f(+\mathbf{V_9}, -\mathbf{V_{11}})$
β-catenin	**-9**, **12**	$\frac{d[\beta\text{-}catenin]}{dt} \approx f(-\mathbf{V_9}, +\mathbf{V_{12}})$

4.2.3 Three exhausted modes

At time $4.7 < t < 8$ *min*, ($M = 3$), see Fig (4.2). The numerical results that will be reported in this section were computed at $t = 6.57$ *min*. The results at $t = 6.57$ *min* are valid thoughout the period in which $M = 3$.

Table 4.25 shows that the three pointed variables are the concentrations of *(β-catenin*/APC* /Axin*/GSK3)*, *(APC/Axin/GSK3)* and *β-catenin**.

Table 4.26 shows that the reactions that contribute the most to the generation of the $4+M = 7$-dim. *SIM* are: (i) reactions 9 and 10 for the first exhausted mode, (ii) reactions 3, $6f$ and $6b$ for the second exhausted mode and (iii) 3, 4, 5, $6f$, 10 and 11 for the third exhausted mode. Given that the *PO* identifies the concentration of *(β-catenin*/APC*/Axin*/GSK3)* (X_9) and the concentration of *(APC/Axin/GSK3)* (X_6) the *PI* identifies the same equilibria as in Section 4.2.2. For the third

Table 4.25: Proteins and protein complexes indicated by *CSP Pointer* in the stimulated state; bold indicates the species pointed the most

M	Proteins and protein complexes	CSP Pointer
1	(**β-catenin*/APC*/Axin*/GSK3)**	**0.82**
	(β-catenin/APC*/Axin*/GSK3)	0.18
2	**(APC/Axin/GSK3)**	**0.60**
	(APC/Axin)	0.40
3	**β-catenin***	**1.00**

exhausted mode the *PO* identifies the concentration of *β-catenin** (X_{10}) and the *PI* indicates that there is an equilibria between reactions V_3, V_4, V_5, V_{6f}, V_{10} and V_{11}.

The reactions that are responsible for the creation of the 7-dimensional *SIM* are accessed by the *Participation Index (PI)* and depicted in Table 4.26. The PI for the first and second exhausted modes indicate again the same equilibria. The pointer for the third exhausted mode identifies *β-catenin** and the PI indicates that there is an equilibria between V_{10} and V_{11}.

Table 4.26: Proteins and protein complexes indicated by *CSP Pointer* are shown in column 3 (most pointed marked bold); reactions exhibiting *Participation Indices* greater than 5% are listed in column 4 (those providing PI's greater than 15% are marked by bold); reactions with + sign equilibrate with those with the - sign.

M	Amplitude of exhausted modes	Proteins and protein complexes	Reactions
1	f^1	(**β-catenin*/APC*/Axin*/GSK3)**, (β-catenin/APC*/Axin*/GSK3)	**9**(0.50), **-10**(0.50)
2	f^2	**(APC/Axin/GSK3)**, (APC/Axin)	**-3**(-0.38), **6f**(0.47), -6b(-0.10)
3	f^3	**β-catenin***	3(0.09), -4(-0.11), 5(0.08), -6f(-0.11),**10**(0.28), **-11**(-0.24)

Table 4.27 lists the significant contributors for the generation of λ_1, λ_2 and λ_3. It is shown that the contribution to the first two eigenvalues are the same reactions as in the case for the two exhausted modes, Section 4.2.2. The contribution to λ_3 is by reaction 11. The reaction has to do with the degradation of *β-catenin** by the destruction complex and the proteasome respectively. This suggests that the speed by which the third fast mode becomes exhausted ($f^3 \approx 0$) has to do with the speed by *β-catenin** is degraded.

Table 4.27: Proteins and protein complexes indicated by *CSP Pointer* are shown in column 3 (most pointed marked bold); reactions exhibiting *Eigenvalue participation index (EPI)* greater than 5% are listed in column 4 (those providing EPI's greater than 15% are marked by bold)

M	Fast eigenvalues	Proteins and protein complexes	Reactions
1	λ_1	(***β*-catenin*/APC*/Axin*/GSK3)**, (β-catenin/APC*/Axin*/GSK3)	**-9**(-0.18), **-10**(-0.82)
2	λ_2	**(APC/Axin/GSK3)**, (APC/Axin)	**-3** (-0.45), **-6f**(-0.40), **+6b**(0.12)
3	λ_3	***β*-catenin***	**-11**(-1.00)

The reactions that contribute to the slow evolution of the system on the 7-dim. *SIM* are depicted in column 2 of Table 4.28. These are reactions that exhibit the largest *II*s. The rate of change of these 8 protein and protein complexes along the *SIM* are determined by the reactions indicated in column 3. The reactions that provide significant contribution to the slow components are 1, 2, 3, 4, 5, $6f$, 9 and 12 that have to do with the (i) activation of *Dsh* by the *Wnt* signal (reaction 1), (ii) deactivation of *Dsh* (reaction 2), (iii) dissociation of *GSK3* from the destruction complex (reaction 3), (iv) phosphorylation of *Axin* and *APC* (reaction 4), (v) dephosphorylation of *Axin* and *APC* (reaction 5), (vi) binding of *GSK3* to the *(APC/Axin)* complex (reaction $6f$), (vii) phosphorylation of *β-catenin* (reaction 9) and (viii) synthesis of *β-catenin* (reaction 12). Given the rising equilibria between reactions 10 and 11, reaction 11 is removed from the slow system. As reactions 10 and 11 start equilibrating equations 3, 4 and 5 start emerging, Table 4.26 so reaction 5 plays again role in the slow system. As time increases reaction 2 is emerging and plays a role too in the slow system.

Table 4.28: Reactions providing non-negligible contribution to selected components of $\mathbf{g}_{slow}$, identified by the *Importance index (II)* Eq.(2.29). Only reactions exhibiting IIs greater than 1% are shown. Those providing IIs greater than 15% are indicated by bold. Reactions with the +(-) sign tend to increase (decrease) the concentration of the related protein or protein and protein complexes.

Proteins and protein complexes	Reactions	Rate of change
Dsh_i	**-1**, **2**	$\frac{d[Dsh_i]}{dt} \approx f(-\mathbf{V_1}, +\mathbf{V_2})$
Dsh_a	**1**, **-2**	$\frac{d[Dsh_a]}{dt} \approx f(+\mathbf{V_1}, -\mathbf{V_2})$
(APC/Axin*/GSK3)*	**-3**, **4**, **-5**, **6f**, 13, -6b	$\frac{d[(APC^*/Axin^*/GSK3)]}{dt} \approx f(-\mathbf{V_3}, +\mathbf{V_4}, -\mathbf{V_5}, +\mathbf{V_{6f}}, +V_{13}, -V_{6b})$
GSK3	1, -2, **3**, **-4**, **5**, **-6f**, 15, 6b	$\frac{d[GSK3]}{dt} \approx f(+V_1, -V_2, +\mathbf{V_3}, -\mathbf{V_4}, +\mathbf{V_5}, -\mathbf{V_{6f}}, +V_{15}, +V_{6b})$
(APC/Axin)	1, -2, **3**, **-4**, **5**, **-6f**, -15, 6b	$\frac{d[(APC/Axin)]}{dt} \approx f(+V_1, -V_2, +\mathbf{V_3}, -\mathbf{V_4}, +\mathbf{V_5}, -\mathbf{V_{6f}}, -V_{15}, +V_{6b})$
APC	**9**, **-12**	$\frac{d[APC]}{dt} \approx f(+\mathbf{V_9}, -\mathbf{V_{12}})$
(β-catenin/APC/Axin*/GSK3)*	**-3**, **4**, **-5**, **6f**, -9, -6b	$\frac{d[(\beta\text{-catenin}/APC^*/Axin^*/GSK3)]}{dt} \approx f(-\mathbf{V_3}, +\mathbf{V_4}, -\mathbf{V_5}, +\mathbf{V_{6f}}, +V_9, -V_{6b})$
β-catenin	**-9**, **+12**	$\frac{d[\beta\text{-catenin}]}{dt} \approx -\mathbf{f}(+\mathbf{V_9}, +\mathbf{V_{12}})$

4.2.4 Four exhausted modes

At time $8.5 < t < 265\ min$, $(M = 4)$, Fig (4.2). The numerical results that will be reported in this section were computed at $t = 192.3\ min$. The results at $t = 192.3\ min$ are valid thoughout the period in which $M = 4$.

Table 4.29 shows that the four pointed variables are the concentrations of *(β-catenin*/APC* /Axin*/GSK3)*, *(APC/Axin/GSK3)*, *β-catenin** and Dsh_i.

Table 4.29: Proteins and protein complexes indicated by *CSP Pointer* in the stimulated state; bold indicates the species pointed the most

M	Proteins and protein complexes	CSP Pointer
1	**(β-catenin*/APC*/Axin*/GSK3)**	**0.79**
	(β-catenin/APC*/Axin*/GSK3)	0.21
2	**(APC/Axin/GSK3)**	**0.65**
	(APC/Axin)	0.34
3	**β-catenin***	**1.00**
4	$\boldsymbol{Dsh_i}$	**0.91**
	Dsh_a	0.09

Table 4.30 shows that the reactions that contribute the most to the generation of the $4+M = 8$-dim. *SIM* are: (i) reactions 9 and 10 for the first exhausted mode, (ii) reactions 3, $6f$ and $6b$ for the second exhausted mode and (iii) 3, 4, 5, $6f$, 10 and 11 for the third exhausted mode. Given that the *PO* identifies the concentration of *(β-catenin*/APC*/Axin*/GSK3)* (X_9) the concentration of *(APC/Axin/GSK3)* (X_6) and the concentration of *β-catenin** the *PI* identifies the same equilibria as in Section 4.2.3. For the fourth exhausted mode the *PO* identifies the concentration of Dsh_i (X_1) and the *PI* indicates that there is an equilibria between reactions V_1, V_2, so that Dsh_i is amenable to *QSSA*, $V_1 - V_2 \approx 0$ since according to Table 3.4 $\dot{X}_1 = -V_1 + V_2$.

Table 4.31 lists the significant contributors for the generation of λ_1, λ_2, λ_3 and λ_4. It is shown that the contribution to the first three eigenvalues are the same reactions as in the section with the three exhausted modes, Section 4.2.3. The contribution to λ_4 is 91% by reaction 1 and 9% by reaction 2 . Reaction 1 has to do with the activation of Dsh_i by the *Wnt*-ligand and reaction 2 has to do with the deactivation of *Dsh*. The speed by which the fourth fast mode is exhausted $f^4 \approx 0$ has to do mainly with the speed that *Wnt*-ligand activates *Dsh*.

The reactions that contribute to the slow evolution of the system on the 8-dim. *SIM* are depicted in column 2 of Table 4.32. These are reactions that exhibit the largest *II*s. The rate of change of these 7 protein and protein complexes along the *SIM* are determined by the reactions indicated in column 3. The reactions that provide significant contribution to the slow components are 1, 2, 3, 4, 5, $6f$, 9 and 12 that have to do with the (i) activation of *Dsh* by the *Wnt* signal (1), (ii) deactivation of *Dsh* (reaction 2), (iii) dissociation of *GSK3* from the destruction complex

Table 4.30: Proteins and protein complexes indicated by *CSP Pointer* are shown in column 3 (most pointed marked bold); reactions exhibiting *Participation Indices* greater than 5% are listed in column 4 (those providing PI's greater than 15% are marked by bold); reactions with + sign equilibrate with those with the - sign.

M	Amplitude of exhausted modes	Proteins and protein complexes	Reactions
1	f^1	(**β-catenin*/APC*/Axin*/GSK3)**, (β-catenin/APC*/Axin*/GSK3)	**9**(0.50), **-10**(-0.50)
2	f^2	**(APC/Axin/GSK3)**, (APC/Axin)	**-3**(-0.40), **6f**(0.48), -6b(-0.08)
3	f^3	**β-catenin***	3(0.06), -4(-0.08), 5(0.08), -6f(-0.08), **10**(0.33), **-11**(-0.33)
4	f^4	$\boldsymbol{Dsh_i}$	**-1**(-0.50), **2**(0.50)

Table 4.31: Proteins and protein complexes indicated by *CSP Pointer* are shown in column 3 (largest pointed marked bold); reactions exhibiting *Eigenvalue participation index (EPI)* greater than 5% are listed in column 4 (those providing EPI's greater than 15% are marked by bold)

M	Fast eigenvalues	Proteins and protein complexes	Reactions
1	λ_1	(**β-catenin*/APC*/Axin*/GSK3)**, (β-catenin/APC*/Axin*/GSK3)	**-9**(-0.20), **-10**(-0.79)
2	λ_2	**(APC/Axin/GSK3)**, (APC/Axin)	**-3**(-0.53), **-6f**(-0.34), **+6b**(0.10)
3	λ_3	**β-catenin***	**-11**(-1.00))
4	λ_4	$\boldsymbol{Dsh_i}$	**-1**(-0.91), -2(0.09)

(reaction 3), (iv) phosphorylation of *Axin* and *APC* (reaction 4), (v) dephosphorylation of *Axin* and *APC* (reaction 5), (vi) binding of *GSK3* to the *(APC/Axin)* complex (reaction $6f$), (vii) phosphorylation of β-*catenin* (reaction 9) and (viii) synthesis of β-*catenin* (reaction 12).

Table 4.32: Reactions providing non-negligible contribution to selected components of $\mathbf{g}_{slow}$, identified by the *Importance index (II)* Eq.(2.29). Only reactions exhibiting IIs greater than 1% are shown. Those providing IIs greater than 15% are indicated by bold. Reactions with the +(-) sign tend to increase (decrease) the concentration of the related protein or protein and protein complexes.

Proteins and protein complexes	Reactions	Rate of change
Dsh_a	**1**, **-2**	$\frac{d[Dsh_a]}{dt} \approx f(+\mathbf{V_1}, -\mathbf{V_2})$
(APC/Axin*/GSK3)*	**-3**, **4**, **-5**, **6f**, -13, -6b	$\frac{d[(APC^*/Axin^*/GSK3)]}{dt} \approx f(-\mathbf{V_3}, +\mathbf{V_4}, -\mathbf{V_5}, +\mathbf{V_{6f}}, -V_{13}, -V_{6b})$
GSK3	**3**, **-4**, **5**, **-6f**, -14, 15, 6b	$\frac{d[GSK3]}{dt} \approx f(+\mathbf{V_3}, -\mathbf{V_4}, +\mathbf{V_5}, -\mathbf{V_{6f}}, -V_{14}, +V_{15}, +V_{6b})$
(APC/Axin)	**3**, **-4**, **5**, **-6f**, 14, -15, 6b	$\frac{d[(APC/Axin)]}{dt} \approx f(+\mathbf{V_3}, -\mathbf{V_4}, +\mathbf{V_5}, -\mathbf{V_{6f}}, +V_{14}, -V_{15}, +V_{6b})$
APC	**9**, **-12**, 13	$\frac{d[APC]}{dt} \approx f(+\mathbf{V_9}, -\mathbf{V_{12}}, +V_{13})$
(β-catenin/APC/Axin*/GSK3)*	**-3**, **4**, **-5**, **6f**, -6b	$\frac{d[(\beta\text{-}catenin/APC^*/Axin^*/GSK3)]}{dt} \approx f(-\mathbf{V_3}, +\mathbf{V_4}, -\mathbf{V_5}, +\mathbf{V_{6f}}, -V_{6b})$
β-catenin	**-9**, **12**	$\frac{d[\beta\text{-}catenin]}{dt} \approx -\mathbf{f}(+\mathbf{V_9}, +\mathbf{V_{12}})$

4.2.5 Five exhausted modes

At time $265 < t < 5000\ min$, $(M = 4)$, Fig (4.2). The numerical results that will be reported in this section were computed at $t = 3511\ min$. The results at $t = 3511\ min$ are valid thoughout the period in which $M = 5$.

Table 4.33 shows that the five pointed variables are the concentrations of *(β-catenin*/APC* /Axin*/GSK3)*, *(APC/Axin/GSK3)*, *β-catenin**, Dsh_i and *(APC/Axin)*.

Table 4.34 shows that the reactions that contribute the most to the generation of the $4 + M = 9$-dim. *SIM* are: (i) reactions 9 and 10 for the first exhausted mode, (ii) reactions 3, $6f$ and $6b$ for the second exhausted mode. Given that the *PO* identifies the concentration of *(β-catenin*/APC*/Axin*/GSK3)* (X_9) and the concentration of *(APC/Axin/GSK3)* (X_6), the *PI* identifies the same equilibria as in Section 4.2.4. For the third exhausted mode the *PO* identifies the concentration of *β-catenin** (X_{10}) and the PI identifies reactions 10 and 11, it follows that the third *CSP* mode relates to the *Quasi Steady State* of the pointed variable, since according to Table 3.4 $\dot{X}_{10} = V_{10} - V_{11}$. For the fourth exhausted mode the *PO*identifies the concentration of Dsh_i (X_1) and the *PI* indicates that there is an equilibria between reactions V_1, V_2, so that Dsh_i is amenable to *QSSA*, $V_1 - V_2 \approx 0$ since according to Table 3.4 $\dot{X}_1 = -V_1 + V_2$. The *PO* for the fifth exhausted mode identifies the concentration of *(APC/Axin)*, *(APC/Axin/GSK3)*, *Axin* and *(APC*/Axin*/GSK3)* and the PI indicates that that V_14 and V_{15} equilibrate.

Table 4.35 lists the significant contributors for the generation of λ_1, λ_2, λ_3, λ_4 and λ_5. It is shown that the contribution to the first four eigenvalues are the same reactions as in the section with the four exhausted modes, Section 4.2.4. The contribution to λ_5 is 15% by reaction 3, 33% by reaction 4, 10% by reaction 5, 19% by reaction $6f$ and 11% by reaction 15. Reactions $3, 5, 6f, 15$ have to do with *Dsh*-mediated release of GSK3 from the destruction complex, dephosphorylation of *(APC*/Axin*/GSK3)*, synthesis of *(APC/Axin/GSK3)* from *(APC/Axin)* and *GSK3* and degradation of *Axin* through *APC* mediation. The speed by which the fifth mode is exhausted $f^5 \approx 0$

Table 4.33: Proteins and protein complexes indicated by *CSP Pointer* in the stimulated state; bold indicates the species pointed the most

M	Proteins and protein complexes	CSP Pointer
1	(**β-catenin*/APC*/Axin*/GSK3)**	**0.75**
	(β-catenin/APC*/Axin*/GSK3)	0.24
2	**(APC/Axin/GSK3)**	**0.65**
	(APC/Axin)	0.34
3	**β-catenin***	**1.00**
4	$\boldsymbol{Dsh_i}$	**0.91**
	Dsh_a	0.09
5	**(APC/Axin)**	**0.34**
	(APC/Axin/GSK3)	**0.27**
	Axin	**0.20**
	(APC*/Axin*/GSK3)	0.18

Table 4.34: Proteins and protein complexes indicated by *CSP Pointer* are shown in column 3 (largest pointed marked bold); reactions exhibiting *Participation Indices* greater than 5% are listed in column 4 (those providing PI's greater than 15% are marked by bold); reactions with + sign equilibrate with those with the - sign.

M	Amplitude of exhausted modes	Proteins and protein complexes	Reactions
1	f^1	(**β-catenin*/APC*/Axin*/GSK3)**, (β-catenin/APC*/Axin*/GSK3)	**9**(0.50), **-10**(0.50)
2	f^2	**(APC/Axin/GSK3)**, (APC/Axin)	**-3**(-0.39), **6f**(0.47), -6b(-0.08)
3	f^3	**β-catenin***	**10**(0.48), **-11**(-0.48)
4	f^4	$\boldsymbol{Dsh_i}$	**-1**(-0.50), **2**(0.50)
5	f^5	**(APC/Axin)**, (APC/Axin/GSK3) Axin, (APC*/Axin*/GSK3)	**-4**(-0.37), **5**(0.37), **14**(0.12), **-15**(-0.12)

has to do with the speed that *(APC/Axin/GSK3)* phosphorylates into *(APC*/Axin*/GSK3)*, with the phosphorylation and dephosphorylation of *Axin* and *APC* and with the degradation of *Axin*.

The reactions that contribute to the slow evolution of the system on the 9-dim. *SIM* are depicted

Table 4.35: Proteins and protein complexes indicated by *CSP Pointer* are shown in column 3 (largest pointed marked bold); reactions exhibiting *Eigenvalue participation index (EPI)* greater than 5% are listed in column 4 (those providing EPI's greater than 15% are marked by bold)

M	Fast eigenvalues	Proteins and protein complexes	Reactions
1	λ_1	(**β-catenin*/APC*/Axin*/GSK3)**, (β-catenin/APC*/Axin*/GSK3)	**-9**(-0.35), **-10**(-0.64)
2	λ_2	**(APC/Axin/GSK3)**, (APC/Axin)	**-3**(-0.53), **-6f**(-0.33), +6b(0.11)
3	λ_3	**β-catenin***	**-11**(-1.00)
4	λ_4	$\boldsymbol{Dsh_i}$	**-1**(-0.91), -2(-0.09)
5	λ_5	**(APC/Axin)** (APC/Axin/GSK3), Axin, (APC*/Axin*/GSK3)	**3**(0.15), **-4**(-0.33), -5(-0.10), **-6f**(-0.19), -15(-0.11)

Table 4.36: Reactions providing non-negligible contribution to selected components of $\mathbf{g}_{slow}$, identified by the *Importance index (II)* Eq.(2.29). Only reactions exhibiting IIs greater than 1% are shown. Those providing IIs greater than 15% are indicated by bold. Reactions with the +(-) sign tend to increase (decrease) the concentration of the related protein or protein and protein complexes.

Proteins and protein complexes	Reactions	Rate of change
Dsh_a	**1**, **-2**	$\frac{d[Dsh_a]}{dt} \approx f(+\mathbf{V_1}, -\mathbf{V_2})$
(APC/Axin*/GSK3)*	9, -12, **14**, **-15**	$\frac{d[(APC^*/Axin^*/GSK3)]}{dt} \approx f(+V_9, -V_{12}, +\mathbf{V_{14}}, -\mathbf{V_{15}})$
GSK3	9, -12, **-14**, **15**	$\frac{d[GSK3]}{dt} \approx f(+V_9, -V_{12}, -\mathbf{V_{14}}, +\mathbf{V_{15}})$
APC	**9**, **-12**, 13	$\frac{d[APC]}{dt} \approx f(+\mathbf{V_9}, -\mathbf{V_{12}}, +V_{13})$
(β-catenin/APC/Axin*/GSK3)*	-9, 12, **14**, **-15**	$\frac{d[(\beta\text{-}catenin/APC^*/Axin^*/GSK3)]}{dt} \approx f(-V_9, +V_{12}, +\mathbf{V_{14}}, -\mathbf{V_{15}})$
β-catenin	**-9, 12**	$\frac{d[\beta\text{-}catenin]}{dt} \approx f(-\mathbf{V_9}, +\mathbf{V_{12}})$

in column 2 of Table 4.36. These are reactions that exhibit the largest *II*s. The rate of change of these 6 protein and protein complexes along the *SIM* are determined by the reactions indicated in column 3. The reactions that provide significant contribution to the slow components are 1, 2, 9, 12, 14 and 15, that have to do with the (i) activation of *Dsh* by the *Wnt* signal (reaction 1), (ii) deactivation of *Dsh* (reaction 2), (iii) phosphorylation of *β-catenin* (reaction 9), (iv) synthesis of *β-catenin* (reaction 12), (v) synthesis of*Axin* (reaction 14) and (vi) degradation of *Axin* (reaction 15). The equilibrium that is generated under the action of the fifth time scale involves reactions 3, 4, 5 and $6f$.

Chapter 5

Conclusions

The detailed model of *Lee et al.* for the *canonical Wnt* pathway was considered here and it was shown that it is amenable to further reduction, beyond the reduction made in [25]. The tools employed in this work to perform this reduction were tools from *Computational Singular Perturbation (CSP)* analysis.

A short description of the *Wnt* pathway was presented first and the various features of the biological mechanism were discussed. The reference and the stimulated state in the *canonical Wnt* pathway were presented schematically and the processes take that place inside the cell were discussed. A brief comparison was made between the two states and some differences were pointed. The general picture that so far has emerged for the function of the *Wnt* pathway is as follows. In the absence of *Wnt* signal (reference state), *β-catenin* is phosphorylated and then leaded to degradation, so that the activation of *Wnt* target genes is suppressed. On the other hand, in the presence of *Wnt* signal (stimulated case), *β-catenin* gets inside the nucleus in order to express the *Wnt* targeted genes.

In order to get a better understanding of the *Wnt* pathway the detailed ODE model that *Lee et al.* introduced in 2003, [25] was analyzed further, on the basis of the multi-scale character of the model. The original model of *Lee et al.* was reduced, by applying four partial equilibrium approximations; see Table 3.4 [25]. This simplification was deemed necessary, since it was known that the four reactions assumed in equilibrium were very fast but the values of the related constants could not be determined. This modified model has been validated extensively against experimental results and is now a reference tool in the relevant research community. The dynamics of the modified model were analyzed in the present work and it was demonstrated that significant gaps develop among its time scales. This feature validated the use of the algorithmic singular perturbation analysis with the *CSP* method.

The modified *Wnt* model was analyzed with the *CSP* algorithm for both states (reference and stimulated) throughout the computational domain. As various points in time, the algorithm identified (i) number of equilibrations that develop under the action of the fast time scales, (ii) the processes (reactions) that participate in these equilibrations, (iii) the the processes (reactions) that generate the exhausted fast time scales, (v) the fast and slow variables and (vi) the processes (reactions) that drive the system within the constraints imposed by the equilibrations.

In the reference state, the exhausted time scales were found to vary monotonically from $M = 1$ to $M = 4$, reaching the largest value after $t \approx 28\ min$. On the other hand, in the stimulated state

the exhausted time scales were found to vary monotonically from $M = 1$ to $M = 5$, reaching the largest value after $t \approx 266\ min$. As the value of M was changing, so were the dimensions and shape of the M-dim. *SIM* and the form of the slow system that governs the flow on the *SIM*.

It was found that the protein and protein complexes that are related to the fast time scales in both the reference and the stimulated states had to do with:

- *(β-catenin*/APC*/Axin*/GSK3)* (X_9) in relation to the fastest time scale,
- *(APC/Axin)*(X_6) in the reference state and *(APC/Axin/GSK3)*(X_4) in the stimulated state in relation to the second fastest time scale,
- *β-catenin** (X_{10}) in relation to the third fast time scale in both states,
- *(APC/Axin/GSK3)* (X_4) in the reference state and Dsh_i (X_1) in the stimulated state in relation to the fourth fastest time scale and
- *(APC/Axin)* (X_6), *(APC/Axin/GSK3)* (X_4), *Axin* (X_{12}) and *(APC*/Axin*/GSK3)* (X_3) in the stimulated state in relation to the fifth fast time scale.

The reactions that participate in the equilibria that form the M-dim. *SIM* were identified as follows:

- phosphorylation of *β-catenin* (reaction 9) and dissociation of phosphorylated *β-catenin* (reaction 10), when $M = 1$ in both states,
- binding of *GSK3* to the *(APC/Axin)* complex (reaction 6f) and dissociation of *GSK3* from the destruction complex (reaction 6b) in the reference state, binding of *GSK3* to the *(APC/Axin)* complex (reaction 6f) and dissociation of *GSK3* from the destruction complex (reactions 6b and 3) in the stimulated when $M = 2$,
- dissociation of *β-catenin** (reaction 10) and degradation of *β-catenin** (reaction 11) when $M = 3$ in both states,
- phosphorylation and dephosphorylation of *Axin* and *APC* (reactions 4 and 5) in the reference state and activation of *Dsh* by *Wnt* signal (reaction 1) and deactivation of *Dsh* (reaction 2) in the stimulated state at time when $M = 4$,
- phosphorylation of *Axin* and *APC* (reaction 4), dephosphotylation of *Axin* and *APC* (reaction 5), synthesis of *Axin* (reaction 14) and degradation of *Axin* (reaction 15) in the stimulated state at time when $M = 5$.

The reactions that contribute to the slow evolution along the M-dimensional *SIM* were identified and the rate of change of the slow protein and protein complexes were presented in the reference and stimulated state, when $M = 1 - 4$ and $M = 1 - 5$, respectively. As the solution reaches the fixed points, see Fig. (3.3)), the reactions that play a significant role in both the reference and the stimulated state are 9 (phosphorylation of *β-catenin*), 12 (synthesis of *β-catenin*), 14 (synthesis of *Axin*) and 15 (degradation of *Axin*). Reactions 1 (activation of *Dsh* by *Wnt*) and 2 (deactivation of *Dsh*) play a significant role only in the simulated state as expected.

Some key features identified by the *CSP* diagnostics are:

- The protein complex *(β-catenin*/APC*/Axin*/GSK3)* relates to the 1^{st} (fastest) *CSP* mode in both states. The related equilibration that is generate relates to the phosphorylation of *β-catenin* and the dissociation of *β-catenin**.

- In both states, the 2^{nd} *CSP* mode relates to the equilibration between the binding of *GSK3* to the *(APC/Axin)* complex (reaction 6f) and the dissociation of *GSK3* from the destruction complex. The dissociation of *GSK3* occurs through (reaction 6b) in the reference state and mainly through (reaction 3) in stimulated state.

- All the reactions that relate directly to *β-catenin* and *β-catenin** or to their complexes are significantly fast; see Fig. 3.2. This set includes (i) reactions 8, 16 and 17, which were assumed in Partial Equilibrium and (ii) reactions 9, 10 and 11, which relate to the 1^{st} and 3^{rd} *CSP* modes, in both the reference and the stimulated state.

- Regarding the 4^{th} *CSP* mode, in the reference state the reactions that equilibrate are phosphorylation and dephosphorylation of *Axin* and *APC*. In the stimulation state the reactions that equilibrate are the activation and deactivation of *Dsh*.

- The 5^{th} *CSP* mode develops only in the stimulated state. The reactions that equilibrate are phosphorylation and dephosphorylation of *Axin* and *APC* (reactions 4 and 5) and synthesis and degradation of *Axin* (reactions 14 and 15). Given the equilibria that develop in the context of (i) the 2^{nd} *CSP* mode between the binding of *GSK3* to the *(APC/Axin)* complex (reaction 6f) and the dissociation of *GSK3* from the destruction complex (reaction 6b) and (ii) one of the four PEAs between the binding of *APC* to *Axin* (reaction 7f) and dissociation of *APC* from the *(APC/Axin)* complex (reaction 7b), the rate by which *Axin* and *APC* phosphorylate and dephosphorylate depends on the rate by which *Axin* is synthesized and degraded.

- Reactions that contribute significantly to the slow evolution in both states were found to be phosphorylation of *β-catenin*, synthesis of *β-catenin*, synthesis of *Axin* and degradation of *Axin*.

Recently, a number of more complex mathematical models for the *Wnt* signaling pathway have emerged, which incorporate components not included in the model by *Lee et al.* [16,35,39,42]. These new models have not been validated as thoroughly, as the model by *Lee et al.* was. Therefore, the multi-scale analysis of these models, along the lines of the present investigation, could provide the required insights on the significance of the new components included in the new models.

Bibliography

[1] R. Aiken. *Stiff Computation.* Oxford Univercsity Press, UK, 1985.

[2] A. Cliffe, F. Hamada, and M. Bienz. A Role of Dishevelled in Relocating Axin to the Plasma Membrane during Wingless Signaling. *Current Biology*, 13(11):960–966, 2003.

[3] F. Cong, L. Schweizer, M. Chamorro, and H. Varmus. Requirement for a nuclear function of β-catenin in Wnt signaling. *Mol Cell Biol*, 23:8462–8470, 2003.

[4] P. Daniel and C. Hans. Wnt control of stem cells and differentiation in the intestinal epithelium. *Experimental Cell Research*, 306(2):357–363, 2005.

[5] D. L. Daniels and W. I. Weis. β-catenin directly displaces Groucho/TLE repressors from Tcf/Lef in Wnt-mediated transcription activation. *Nat Struct Mol Biol*, 12:364–371, 2005.

[6] D. M. Eisenmann. Wnt signaling. Wormbook, e.d. The online review of Caenorhabditis elegans biology, 2005. `http://www.wormbook.org`.

[7] R. H. Giles, J. H. van Es, and H. Clevers. Caught up in a Wnt storm: Wnt signaling in cancer. *Biochemica et Biophysica Acta - Reviews on Cancer*, 1653(1):1–24, 2003.

[8] D. Goussis and G. Skevis. Nitrogen chemistry controlling steps in methane-air premixed flames. pages 650–653, 2005.

[9] D. A. Goussis and S. H. Lam. A study of homogeneous methanol oxidation kinetics using CSP. *Symposium (International) on Combustion*, 24(1):113 – 120, 1992.

[10] D. A. Goussis and M. Valorani. An efficient iterative algorithm for the approximation of the fast and slow dynamics of stiff systems. *Comp. Physics*, 214:317–325, 2006.

[11] N.-C. Ha, T. Tonozuka, J. L. Stamos, H.-J. Choi, and W. I. Weis. Mechanism of Phosphorylation-Dependent Binding of APC to β-Catenin and Its Role in β-Catenin Degradation. *Molecular Cell*, 15(4):511–521, 2004.

[12] R. Heinrich. Mathematical modelling of the wnt-pathway. In *Systems Biology*, volume 13, pages 259–275. Springer Berlin Heidelberg, 2005.

[13] C. Y. Janda, D. Waghray, A. M. Levin, C. Thomas, and K. C. Garcia. Structural basis of Wnt recognition by Frizzled. *Science*, 337:59–64, 2012.

[14] J. Kevorkian and J. Cole. *Perturbation Methods in Applied Mathematics*. Springer Verlag, New York, 1980.

[15] H. Kitano. Systems Biology: A Brief Overview. *Science*, 295(5560):2533, 2002.

[16] Y. Kogan, K. E. HaleviTobias, G. Hochman, A. K. Baczmanska, L. Leyns, and Z. Agur. A new validated mathematical model of the wnt signalling pathway predicts effective combinational therapy by sfrp and dkk. *Biochemical Journal*, 444(1):115–125, 2012.

[17] P. D. Kourdis and D. A. Goussis. Glycolysis in saccharomyces cerevisiae: Algorithmic exploration of robustness and origin of oscillations. *Mathematical Biosciences*, 243:190–214, 2013.

[18] P. D. Kourdis, R. Steuer, and D. A. Goussis. Physical understanding of complex multiscale biochemical models via algorithmic simplification: Glycolysis in Saccharomyces cerevisiae. *Physica D: Nonlinear Phenomena*, 239(18):1798–1817, 2010.

[19] R. Krüger and R. Heinrich. Model Reduction and Analysis of Robustness for the Wnt/β-Catenin Signal. *Genome Informatics*, 15(1):138–148, 2004.

[20] S. H. Lam. Using CSP to understand complex chemical kinetics. *Combustion Science and Technology*, 89:375–404, 1993.

[21] S. H. Lam and D. A. Coussis. Conventional asymptotics and computational singular perturbation for simplified kinetics modelling. In *Reduced Kinetic Mechanisms and Asymptotic Approximations for Methane-Air Flames*, volume 384, pages 227–242. Springer Berlin Heidelberg, 1991.

[22] S. H. Lam and D. A. Goussis. Understanding complex chemical kinetics with computational singular perturbation. *Proc. Comb. Inst.*, 22:931–941, 1988.

[23] S. H. Lam and D. A. Goussis. The CSP method for simplifying kinetics. *Intl. J. of Chem. Kinetics*, 26:461–486, 1994.

[24] E. Lee, A. Salic, and M. W. Kirschner. Physiological regulation of β-catenin stability by Tcf3 and CK1ϵ. *J Cell Biol*, 154:983–994, 2001.

[25] E. Lee, A. Salic, R. Krüger, R. Heinrich, and M. W. Kirschner. The Roles of APC and Axin Derived from Experimental and Theoretical Analysis of the Wnt Pathway. *PLoS Biol*, 1:116–132, 2003.

[26] C. Liu, Y. Li, M. Semenov, C. Han, G.-H. Baeg, Y. Tan, Z. Zhang, X. Lin, and X. He. Control of β-Catenin Phosphorylation/Degradation by a Dual-Kinase Mechanism. *Cell*, 108(6):837–847, 2002.

[27] B. Lloyd-Lewis, A. G. Fletcher, T. C. Dale, and H. M. Byrne. Toward a quantitative understanding of the Wnt/β-catenin pathway through simulation and experiment. *Wiley Interdisciplinary Reviews: Systems Biology and Medicine*, 5(4):391–407, 2013.

[28] W. Materi and D. S. Wishart. Computational systems biology in drug discovery and development: methods and applications. *Drug Discovery Today*, 12(78):295 – 303, 2007.

[29] G. Mirams, H. Byrne, and J. King. A multiple timescale analysis of a mathematical model of the Wnt/β-catenin signalling pathway. *Journal of Mathematical Biology*, 60(1):131–160, 2010.

[30] K. Orford, C. Crockett, J. Jensen, A. Weissman, and S. Byers. Serine phosphorylation-regulated ubiquitination and degradation of β-catenin. *J Biol Chem*, 272:24735–24738, 1997.

[31] J. M. Peters, R. M. McKay, J. P. McKay, and J. M. Graff. Casein kinase I transduces Wnt signals. *Nature*, 401:345–350, 1999.

[32] T. Reya and H. Clevers. Wnt signalling in stem cells and cancer. *Nature*, 434(1):1–24, 2005.

[33] B. Rubinfeld, D. Tice, and P. Polakis. Axin-dependent phosphorylation of the adenomatous polyposis coli protein mediated by casein kinase 1ϵ. *J Biol Chem*, 276:39037–39045, 2001.

[34] A. Salic, E. Lee, L. Mayer, and M. W. Kirschner. Control of β-Catenin Stability: Reconstitution of the Cytoplasmic Steps of the Wnt Pathway in Xenopus Egg Extracts. *Molecular Cell*, 5(3):523–532, 2000.

[35] Y. Schmitz, O. Wolkenhauer, and K. Rateitschak. Nucleo-cytoplasmic shuttling of {APC} can maximize catenin/tcf concentration. *Journal of Theoretical Biology*, 279(1):132 – 142, 2011.

[36] S. Schnell, R. Grima, and P. Maini. Multiscale modeling in biology. *American Scientist*, 95(2):134–142, 2007.

[37] N. Tolwinski and E. Wieschaus. Rethinking WNT signaling. *Trends in Genetics*, 20(4):177–181, 2004.

[38] M. Valorani, D. A. Goussis, F. Creta, and H. N. Najm. Higher order corrections in the approximation of low-dimensional manifolds and the construction of simplified problems with the CSP method . *Journal of Computational Physics*, 209(2):754–786, 2005.

[39] I. M. van Leeuwen, H. M. Byrne, O. E. Jensen, and J. R. King. Elucidating the interactions between the adhesive and transcriptional functions of β-catenin in normal and cancerous cells. *Journal of Theoretical Biology*, 247(1):77 – 102, 2007.

[40] F. Verhulst. *Methods and Applications of Singular Perturbations*. Springer Verlag, New York, 2000.

[41] F. Verhulst. Periodic solutions and slow manifolds. *International Journal of Bifurcation and Chaos*, 17(8):2533, 2007.

[42] C. Wawra, M. Khl, and H. A. Kestler. Extended analyses of the wnt/-catenin pathway: Robustness and oscillatory behaviour. {*FEBS*} *Letters*, 581(21):4043 – 4048, 2007.

[43] M. Wynn, S. Merajver, and S. Schnell. Unraveling the complex regulatory relationships between metabolism and signal transduction in cancer. In *Advances in Systems Biology*, volume 736, pages 179–189. Springer New York, 2012.

[44] A. Zagaris, H. Kaper, and T. Kaper. Analysis of the computational singular perturbation reduction method for chemical kinetics. *Journal of Nonlinear Science*, 14(1):59–91, 2004.